Novel, Potent, and Radio-Iodinatable Somatostatin Receptor 1 (sst_1) Selective Analogues

Judit Erchegyi,[⊥,†] Renzo Cescato,[⊥,§] Christy Rani R. Grace,[⊥,‡] Beatrice Waser,[§] Véronique Piccand,[§] Daniel Hoyer,[∥] Roland Riek,[‡] Jean E. Rivier,*[,†] and Jean Claude Reubi[§]

The Clayton Foundation Laboratories for Peptide Biology, Structural Biology Laboratory, The Salk Institute for Biological Studies, 10010 North Torrey Pines Road, La Jolla, California 92037, Division of Cell Biology and Experimental Cancer Research, Institute of Pathology, University of Berne, Berne, CH 3010, Switzerland, Psychiatry/Neuroscience Research, WSJ-386/745, Novartis Institutes for Biomedical Research, Basel, CH 4002 Basel, Switzerland

Received October 17, 2008

The proposed sst_1 pharmacophore (*J. Med. Chem.* **2005**, *48*, 523−533) derived from the NMR structures of a family of mono- and dicyclic undecamers was used to design octa-, hepta-, and hexamers with high affinity and selectivity for the somatostatin sst_1 receptor. These compounds were tested for their in vitro binding properties to all five somatostatin (SRIF) receptors using receptor autoradiography; those with high SRIF receptor subtype 1 (sst_1) affinity and selectivity were shown to be agonists when tested functionally in a luciferase reporter gene assay. Des-AA$^{1,4-6,10,12,13}$-[DTyr^2,DAgl(NMe,2naphthoyl)^8,IAmp^9]-SRIF-Thr-NH$_2$ (**25**) was radio-iodinated (^{125}I-**25**) and specifically labeled sst_1-expressing cells and tissues. 3D NMR structures were calculated for des-AA$^{1,4-6,10,12,13}$-[DPhe^2,DTrp^8,IAmp^9]-SRIF-Thr-NH$_2$ (**16**), des-AA$^{1,2,4-6,10,12,13}$-[DAgl-(NMe,2naphthoyl)^8,IAmp^9]-SRIF-Thr-NH$_2$ (**23**), and des-AA$^{1,2,4-6,10,12,13}$-[DAgl(NMe,2naphthoyl)^8,IAmp^9,Tyr^{11}]-SRIF-NH$_2$ (**27**) in DMSO. Though the analogues have the sst_1 pharmacophore residues at the previously determined distances from each other, the positioning of the aromatic residues in **16**, **23**, and **27** is different from that described earlier, suggesting an induced fit mechanism for sst_1 binding of these novel, less constrained sst_1-selective family members.

Introduction

Somatostatin (SRIF[a]) is a cyclic tetradecapeptide widely distributed throughout the body with important regulatory effects (mostly inhibitory) on a variety of endocrine and exocrine functions. It was originally isolated from the hypothalamus and characterized in 1973.[2,3] Somatostatin is also found in the gut, pancreas, in the nervous system, and in various exocrine and endocrine glands. Somatostatin inhibits the release of growth hormone from the anterior pituitary, insulin and glucagon from the pancreas, and gastrin from the gastrointestinal tract. It also has antiproliferative activity and acts as a neurotransmitter or neuromodulator in the brain.[4–7a]

SRIF interacts with five specific receptor subtypes (sst_1−sst_5) that have been cloned and characterized, all belonging to the G-protein-coupled receptor family.[8–10] Cell lines recombinantly expressing these cloned receptors are available to test SRIF analogues for binding affinity, selectivity, and functional effects.[7,11–13] So far, only sst_2 and sst_5 receptors have been clearly linked to specific physiological functions.[14,15] For sst_1 receptors, however, the cellular localization as well as the distinct functions are still not fully understood, similarly to our current lack of knowledge of sst_3 or sst_4 receptor function and physiology.

Sst_1 receptors have been found in human cerebral cortex,[16] human retina,[17] neuroendocrine cells,[14] endothelial cells of human blood vessels (arteries and veins),[18] and human tumors.[19–24] According to Lanneau[25] and Olias,[14] sst_1 receptors are involved in the intrahypothalamic regulation of growth hormone (GH) secretion. The studies of Kreienkamp et al. suggested an important role for sst_1 in the control of basal GH release in somatotrophs.[26] Zatelli et al. have demonstrated that sst_1-selective activation inhibits hormone secretion and cell viability in GH- and prolactin-secreting adenomas in vitro and suggested that somatostatin analogues with affinity for sst_1 receptors may be useful to control hormone hypersecretion and reduce neoplastic growth of pituitary adenomas.[27] Sst_1 receptor activation also modulates somatostatin release in basal ganglia.[28] In hypothalamic, basal ganglia, and retinal functions, the sst_1 receptor appears to act as an inhibitory autoreceptor located on somatostatin neurons, whereas in the hippocampus, such a role is still based on circumstantial evidence.

Sst_1-selective analogues could possibly play a role in various diseases. For instance, retinal disease therapeutics has been a suggested indication for sst_1.[17,28–30] Recently, an sst_1 antagonist was shown to promote social interactions, reduce aggressive

* To whom correspondence should be addressed. Phone: (858) 453-4100. Fax: (858) 552-1546. E-mail: jrivier@salk.edu.
† The Clayton Foundation Laboratories for Peptide Biology.
‡ Structural Biology Laboratory, The Salk Institute for Biological Studies.
§ Division of Cell Biology and Experimental Cancer Research, Institute of Pathology, University of Berne.
∥ Psychiatry/Neuroscience Research, WSJ-386/745, Novartis Institutes for Biomedical Research.
⊥ These authors contributed equally.

[a] Abbreviations: The abbreviations for the common amino acids are in accordance with the recommendations of the IUPAC-IUB Joint Commission on Biochemical Nomenclature (Eur. J. Biochem., **1984**, *138*, 9−37). The symbols represent the L-isomer except when indicated otherwise. Additional abbreviations: AA, amino acid; Agl, aminoglycine; ATP, adenosine 5′-triphosphate; Boc, *tert*-butoxycarbonyl; Bzl, benzyl; Bzl(3Br), 3-bromobenzyl; cAMP, 3′,5′-cyclic adenosine monophosphate; Cbm, carbamoyl; CM, chloromethyl; CZE, capillary zone electrophoresis; DIC, *N*,*N*′-diisopropylcarbodiimide; DIPEA, diisopropylethylamine; DMEM, Dulbecco's modified Eagle's medium; DMF, dimethylformamide; DQF-COSY, double quantum filtered correlation spectroscopy; Fmoc, 9-fluorenylmethoxycarbonyl; HEPES, 4-(2-hydroxyethyl) piperazine-1-ethansulfonic acid; hhLys, homohomolysine; HOBt, 1-hydroxybenzotriazole; IAmp, 4-(*N*-isopropyl)-aminomethylphenylalanine; MBHA, 4-methylbenzhydrylamine; Mob, 4-methoxybenzyl; Nal, 3-(2-naphthyl)-alanine; NMP, *N*-methylpirrolidinone; NOESY, nuclear Overhauser enhancement spectroscopy; PBS, phosphate buffered saline; rmsd, root-mean-square deviation; ROESY, rotating frame nuclear Overhauser enhancement spectroscopy; SRE, serum response element; SRIF, somatostatin; SRIF-28, somatostatin-28; sst_s, SRIF receptors; TEA, triethylamine; TEAP, triethylammonium phosphate; TFA, trifluoroacetic acid; TOCSY, total correlation spectroscopy; Z(2Br), 2-bromobenzyloxycarbonyl; Z(2Cl), 2-chlorobenzyloxycarbonyl.

10.1021/jm801314f CCC: $40.75
Published on Web 04/07/2009

behavior, and stimulate learning.[31,32] Matrone et al. demonstrated the role of sst_1-selective analogues in mediating the inhibitory effect of SRIF on growth hormone secreting pituitary tumors. They suggested that the sst_1-selective analogues might represent a further useful approach for the treatment of acromegaly in patients resistant or partially responsive to octreotide-LAR or lanreotide treatment in vivo.[33] It has also been reported that in medullary thyroid carcinoma, calcitonin secretion and gene expression can be reduced by treatment with sst_1-selective agonists by the reduction of cAMP response element binding phosphorylation, suggesting that potent sst_1-selective agonists could have a therapeutic role in medullary thyroid carcinoma.[34,35] Furthermore, because sst_1-selective agonists were able to inhibit endothelial activities, a potential therapeutic utility for administration of sst_1-selective agonists in the proliferative diseases involving angiogenesis has been suggested.[18]

Although numerous reports on the localization, physiological, and therapeutic functions of sst_1 receptors have been published, it is still not clear which is the main sst_1 receptor function and the main sst_1 related pathology. The design of more potent and more (>100-fold) sst_1-selective agonists and antagonists with radio-labelable properties for in vitro binding assays and in vivo scintigraphy studies as well as greater metabolic stability in biological fluids than the native hormone could help to further understand sst_1-related biology and pathobiology.

Originally, we had identified the first generation of a peptidic scaffold with selected amino acids (AA) deletions (des-$AA^{1,2,5}$-SRIF) that in combination with DTrp at position 8 and 4-(*N*-isopropyl)-aminomethylphenylalanine (IAmp) at position 9 yielded des-$AA^{1,2,5}$-[$DTrp^8$,$IAmp^9$]-SRIF (CH-275)[36] (**2**) (Table 1), a SRIF agonist that was 30-fold more selective for sst_1 versus $sst_{2/4/5}$ and 10-fold versus sst_3, respectively.[36] Our standard drug design approaches led to additional very potent sst_1-selective mono- and dicyclic undecapeptides des-$AA^{1,2,5}$-[$DTrp^8$,$IAmp^9$,Tyr^{11}]-SRIF (**3**),[37] des-$AA^{1,2,5}$-[$DTrp^8$,$IAmp^9$,$ITyr^{11}$]-SRIF (**4**),[37] des-$AA^{1,2,5}$-[$DTrp^8$,$IAmp^9$,$ITyr^{11}$]-Cbm-SRIF (**5**),[1] des-$AA^{1,2,5}$-cyclo(7−12)[Glu^7,$DTrp^8$,$IAmp^9$,$ITyr^{11}$,$hhLys^{12}$]-SRIF (**6**),[38] and des-$AA^{1,2,5}$-[DAgl(NMe,2naphthoyl)^8,$IAmp^9$, Tyr^{11}]-SRIF (**7**)[39] Table 1.[1,37–40]

In several drug design studies of different hypothalamic releasing hormones (gonadotropin-releasing hormone (GnRH),[41] corticotropin-releasing factor (CRF),[42] (SRIF[37,43,44]), we had demonstrated that substitutions of natural amino acids with betidamino acids were compatible with biological activity. Betidamino acids are monoacylated derivatives of α-aminoglycine. The synthesis of α-Fmoc,*β*-Boc-aminoglycine was originally described by Qasmi et al.,[45] and the synthesis of the methylated derivatives was published by our group.[46] As we demonstrated earlier, the substitution of $DTrp^8$ by DAgl(NMe,2naphthoyl)^8 in the undecamer scaffold[37] (**3** versus **7**, Table 1) had resulted in a 5-fold increase in binding affinity at sst_1.[39]

Here, we describe the rational design and optimization of a novel class of peptidic somatostatin sst_1-selective analogues derived from the use of our published sst_1-pharmacophore model.[1]

Results and Discussion

Peptide Synthesis. All analogues shown in Table 1 were synthesized either manually or automatically on a 4-methylbenzhydrylamine (MBHA) or chloromethylated (CM) resin using the Boc-strategy and *N*,*N*′-diisopropylcarbodiimide (DIC)/1-hydroxybenzotriazole (HOBt) for amide bond formation.

We used an unresolved aminoglycine (Agl) derivative Fmoc-D/LAgl(NMe,Boc)-OH[46,47] as a template for the introduction of a betidamino acid in the scaffolds (des-$AA^{1,4-6,10,12,13}$-SRIF-Thr/Nal-NH_2, des-$AA^{1,2,4-6,10,12,13}$-SRIF-Thr/Nal-NH_2, and des-$AA^{1,2,4-6,10,12,13}$-SRIF-NH_2), which resulted in diastereomeric mixtures that were separated by RP-HPLC[48–50] and were fully characterized. The absolute configuration of the Agl residue in the diastereomers was deduced from enzymatic hydrolysis studies with aminopeptidase M and proteinase K, respectively. Comparison of the enzymatic cleavage patterns of the diastereomers showed that the LAgl-containing analogue was hydrolyzed while the DAgl-containing analogue was not.[50]

The peptide resins were treated with anhydrous hydrogen fluoride in the presence of scavengers (anisole and dimethylsulfide) to liberate the fully deblocked crude peptides. Cyclization of the cysteines was mediated by iodine in an acidic milieu. Purification was achieved using multiple RP-HPLC steps.[49] Analytical RP-HPLC,[49] capillary zone electrophoresis (CZE),[51] and mass spectrometry were used to determine the purity and identity of the analogues.

NMR Studies. The NMR samples of **16**, **23**, and **27** were prepared by dissolving 2.5 mg of the peptide in 500 μL of DMSO-d_6. Assignment of the various proton resonances was carried out using the standard procedure using DQF-COSY, TOCSY, and NOESY experiments. Though **16** showed a single set of resonances for all the protons, two sets of resonances were observed for most of the protons for **23** and **27** in the ratio 60:40, except for the HN and αH resonances of $IAmp^9$. This is due to the *cis*/*trans* isomerization of the amide bond present in the side chain of the betidamino acid DAgl at position 8 of **23** and **27**, as reported earlier.[52] Almost complete assignment of the chemical shifts of the various proton resonances is carried out for **16**, **23**, and **27** and is shown in parts A−C of Table 2. Amide resonances of Cys^3 were not observed for **23** and **27** in the NMR spectra due to fast exchange with the solvent.

A reasonably large number of experimental NOEs is observed for the three analogues in the NOESY spectrum measured with a mixing time of 100 ms, leading to over 70 meaningful distance restraints per analogue (Table 3, Figure 1). For all analogues, structural restraints from NOEs were used as input for the structure calculation with the program CYANA,[53] followed by restrained energy minimization using the program DISCOVER.[54] The resulting bundle of 20 conformers per analogue represents the 3D structure of each analogue. For each analogue, the small residual violations in the distance constraints only for the 20 refined conformers (Table 3) and the coincidence of experimental NOEs and short interatomic distances (data not shown) indicate that the input data represent a self-consistent set and that the restraints are well satisfied in the calculated conformers (Table 3). The deviations from ideal geometry are minimal, and similar energy values were obtained for all 20 conformers of each analogue. The quality of the structures determined is reflected by the small backbone rmsd values relative to the mean coordinates of ∼0.5 Å (see Table 3 and Figure 2).

Three-Dimensional Structure of H-$DPhe^2$-c[Cys^3-Phe^7-$DTrp^8$-$IAmp^9$-Phe^{11}-Cys^{14}]-Thr^{15}-NH_2 (16). Analogue **16** binds selectively to sst_1 with moderately high affinity (IC_{50} ∼ 30 nM). It differs from octreotide by $IAmp^9$, Phe^{11}, and Thr^{15}-NH_2, and the 3D NMR structure shows that the backbone has a *β*-turn of type III' around $DTrp^8$ and $IAmp^9$ (Figure 2A, Table 4). In all of the calculated 20 conformers, there is a hydrogen bond between the amide protons of Phe^{11} to the carbonyls of Phe^7

Publication Date (Web): April 7, 2009 | doi: 10.1021/jm801314f

Table 1. Physicochemical Properties and sst$_{1-5}$ Binding Affinities (IC$_{50}$s, nM) of sst$_1$-Selective Analogues and Control Peptides[a]

		purity (%)		MS[d]		IC$_{50}$ nM[e]					
	compd	HPLC[b]	CZE[c]	M (mono) calcd	MH$^+$ (mono) obs	sst$_1$	sst$_2$	sst$_3$	sst$_4$	sst$_5$	luciferase assay
1	SRIF-28	98	93	1636.72	1637.70	2.9 ± 0.2	2.6 ± 0.11	4.3 ± 0.39	2.9 ± 0.2	2.9 ± 0.24	agonist
2	des-AA^{1,2,5}-[DTrp^8,IAmp^9]-SRIF[36]	94	97	1484.66	1485.5	31 ± 13	>1K	540; 150	>1000	>1K	
3	des-AA^{1,2,5}-[DTrp^8,IAmp^9,Tyr^{11}]-SRIF[37]	98	97	1500.66	1501.5	17 ± 6.0	>1K	>1K	>1K	>1K	
4	des-AA^{1,2,5}-[DTrp^8,IAmp^9,ITyr^{11}]-SRIF[37]	94	96	1626.55	1627.5	3.6 ± 0.69	>1K	>1K	>1K	>1K	
5	des-AA^{1,2,5}-[DTrp^8,IAmp^9,ITyr^{11}]-Cbm-SRIF[1]	91	97	1669.56	1670.56	2.5 ± 0.2	>1K	618 ± 125	>1K	>1K	
6	des-AA^{1,2,5}-cyclo(7−12)[Glu^7,DTrp^8,IAmp^9, ITyr^{11},hhLys^{12}]-SRIF[38]	98	98	1645.57	1646.50	6.1 ± 0.6	>1K	>1K	>1K	>1K	
7	des-AA^{1,2,5}-[DAgl(NMe,2naphthoyl)^8,IAmp^9,Tyr^{11}]-SRIF[39]	89	93	1554.67	1555.70	3.3 ± 1.0	>1K	>1K	562 ± 135	>1K	
8	des-AA^{1,2,4,5,12,13}-[DTrp^8]-SRIF[50]	95	98	1078.45	1078.90	27 ± 3.4	41 ± 8.7	13 ± 3.2	1.8 ± 0.7	46 ± 27	
9	des-AA^{1,2,4,5,12,13}-[DTrp^8,IAmp^9]-SRIF	98	98	1168.58	1169.5	>1K	>1K	>1K	>1K	>1K	
10	des-AA^{1,2,5,12,13}-[DTrp^8,IAmp^9]-SRIF	99	99	1296.58	1297.1	189 ± 31	>1K	789 ± 231	932 ± 125	>1K	
11	des-AA$^{1,4-6,11-13}$-[DPhe^2,DTrp^8]-SRIF-Thr-NH$_2$	95	99	1031.4	1032.0	>1K	1.9 ± 0.33	39 ± 14	>1K	5.1 ± 1.1	
12	des-AA$^{1,4-6,11-13}$-[Cpa^2,DCys^3,Tyr^7,DTrp^8]-SRIF-2Nal-NH$_2$[60]	99	99	1177.43	1178.43	>1K	5.7 ± 1.5	112 ± 32	296 ± 19	218 ± 63	
13	des-AA$^{1,4-6,11-13}$-[Cpa^2,DCys^3,Tyr^7,DTrp^8,IAmp^9]-SRIF-2Nal-NH$_2$	98	98	1267.48	1268.45	>1K	240; 665	300; 234	>1K	>1K	
14	des-AA$^{1,4-6,12,13}$-[Tyr^2,DTrp^8,IAmp^9]-SRIF-Thr-NH$_2$	98	98	1284.55	1285.6	150; 186	>1K	60; 284	>1K	>1K	
15	des-AA$^{1,2,4-6,10,12,13}$-[DTrp^8,IAmp^9]-SRIF-Thr-NH$_2$	99	99	1020.45	1021.51	108; 120	>1K	>1K	585; 250	>1K	
16	des-AA$^{1,4-6,10,12,13}$-[DPhe^2,DTrp^8,IAmp^9]-SRIF-Thr-NH$_2$	99	99	1167.50	1168.38	41; 14	>1K	448; 72	1349; 252	>1K	
17	des-AA$^{1,2,4-6,10,12,13}$-[DTrp^8,IAmp^9,ITyr^{11}]-SRIF-Thr-NH$_2$	99	99	1162.33	1163.24	591; 889	>1K	701; 989	468; 1273	>1K	
18	des-AA$^{1,4-6,10,12,13}$-[DPhe^2,DTrp^8,IAmp^9,ITyr^{11}]-SRIF-Thr-NH$_2$	99	98	1309.40	1310.43	449; 565	>1K	514; 864	>1K	>1K	
19	des-AA$^{1,2,4-6,10,12,13}$-[DCys^3,DTrp^8,IAmp^9,ITyr^{11}]-SRIF-2Nal-NH$_2$	97	98	1258.36	1259.33	356; 689	>1K	162; 438	329; 489	>1K	
20	des-AA$^{1,4-6,10,12,13}$-[Cpa^2,DCys^3,DTrp^8,IAmp^9,ITyr^{11}]-SRIF-2Nal-NH$_2$	95	95	1439.39	1440.21	>1K	>1K	>1K	>1K	>1K	
21	des-AA$^{1,4-6,10,12,13}$-[Cpa^2,DCys^3,DAgl(NMe,2naphthoyl)^8]-SRIF-2Nal-NH$_2$	98	96	1262.46	1262.3	20; 29	100; 881	17; 23	71; 72	9.9; 29	
22	des-AA$^{1,4-6,10,12,13}$-[Cpa^2,DCys^3,LAgl(NMe,2naphthoyl)^8]-SRIF-2Nal-NH$_2$	91	93	1262.46	1262.3	>1K	>1K	312	>1K	>1K	
23	des-AA$^{1,2,4-6,10,12,13}$-[DAgl(NMe,2naphthoyl)^8,IAmp^9]-SRIF-Thr-NH$_2$	94	95	1074.45	1075.60	1.0 ± 0.25	>1K	681 ± 52	95 ± 18	>1K	agonist
24	des-AA$^{1,2,4-6,10,12,13}$-[LAgl(NMe,2naphthoyl)^8,IAmp^9]-SRIF-Thr-NH$_2$	97	98	1074.45	1075.59	37; 42	>1K	848; 253	833; 525	>1K	
25	des-AA$^{1,4-6,10,12,13}$-[DTyr^2,DAgl(NMe,2naphthoyl)^8,IAmp^9]-SRIF-Thr-NH$_2$	99	99	1237.52	1238.52	0.19 ± 0.04	>1K	158 ± 14	27 ± 7.5	>1K	agonist
26	des-AA$^{1,4-6,10,12,13}$-[DTyr^2,LAgl(NMe,2naphthoyl)^8,IAmp^9]-SRIF-Thr-NH$_2$	99	99	1237.52	1238.25	124; 97	>1K	>1K	>1K	>1K	
27	des-AA$^{1,2,4-6,10,12,13}$-[DAgl(NMe,2naphthoyl)^8,IAmp^9,Tyr^{11}]-SRIF-NH$_2$	80	87	989.40	990.18	4.7; 7.3	>1K	252; 381	695; 266	>1K	agonist
28	des-AA$^{1,2,4-6,10,12,13}$-[LAgl(NMe,2naphthoyl)^8,IAmp^9,Tyr^{11}]-SRIF-NH$_2$	81	94	989.40	990.18	530; 631	>1K	>1K	>1K	>1K	
29	des-AA$^{1,2,4-6,10,12,13}$-[DCys^3,DAgl(NMe,2naphthoyl)^8,IAmp^9]-SRIF-2Nal-NH$_2$	91	93	1170.48	1171.70	1.2 ± 0.54	>1K	112 ± 23	63 ± 32	181 ± 5	agonist
30	des-AA$^{1,2,4-6,10,12,13}$-[DCys^3,LAgl(NMe,2naphthoyl)^8,IAmp^9]-SRIF-2Nal-NH$_2$	98	85	1170.48	1171.50	267; 316	>1K	329; 729	535; 214	279; 635	
31	des-AA$^{1,4-6,10,12,13}$-[Tyr^2,DCys^3,DAgl(NMe,2naphthoyl)^8,IAmp^9]-SRIF-2Nal-NH$_2$	81	87	1333.55	1334.81	8.2 ± 4.9	>1K	410 ± 114	270 ± 122	>1K	agonist
32	des-AA$^{1,4-6,10,12,13}$-[Tyr^2,DCys^3,LAgl(NMe,2naphthoyl)^8,IAmp^9]-SRIF-2Nal-NH$_2$	73	86	1333.55	1334.61	189; 365	>1K	463; 1169	>1K	>1K	
33	des-AA^{1,5}-[Tyr^2,DTrp^8,IAmp^9]-SRIF[37]	97	97	1647.73	1648.8	14 ± 3	>1K	>1K	>1K	>1K	agonist
34	des-AA$^{1,4-6,10,12,13}$-[D^{nat}ITyr^2,DAgl(NMe,2naphthoyl)^8,IAmp^9]-SRIF-Thr-NH$_2$	88	99	1363.41	1364.29	0.8 ± 0.14	>1K	344 ± 123	45 ± 6.7	>1K	

[a] Structure of SRIF: (cyclo3−14)H-Ala^1-Gly^2-Cys^3-Lys^4-Asn^5-Phe^6-Phe^7-Trp^8-Lys^9-Thr^{10}-Phe^{11}-Thr^{12}-Ser^{13}-Cys^{14}-OH. [b] Percent purity determined by HPLC using buffer system: A = TEAP (pH 2.5) and B = 60% CH_3CN/40% A with a gradient slope of 1% B/min, at flow rate of 0.2 mL/min on a Vydac C_{18} column (0.21 cm × 15 cm, 5 μm particle size, 300 Å pore size). Detection at 214 nm. [c] Capillary zone electrophoresis (CZE) was done using a Beckman P/ACE System 2050 controlled by an IBM Personal System/2 model 50Z and using a ChromJet integrator. Field strength of 15 kV at 30 °C, mobile phase: 100 mM sodium phosphate (85:15, H_2O:CH_3CN) pH 2.50, on a Supelco P175 capillary (363 μm OD × 75 μm id × 50 cm length). Detection at 214 nm. [d] The calculated *m*/*z* of the monoisotope compared with the observed $[M + H]^+$ monoisotopic mass. [e] The IC$_{50}$ values (in nM) were derived from competitive radioligand displacement assays reflecting the affinities of the analogues for the five cloned somatostatin receptors using the nonselective ^{125}I-[Leu^8,DTrp^{22},Tyr^{25}]SRIF-28 as radioligand. Mean value ± SEM when $n \geq 3$. When $n < 3$, individual values of two assays are listed. 1K corresponds to 1000.

Table 2. Chemical Shifts (in ppm) of **16**, **23**, and **27** in DMSO-d_6

residue		NH	αH	βH	others
			(A) Chemical Shifts (in ppm) of **16** in DMSO-d_6		
DPhe^2		8.00	4.19	3.26, 2.97	QD: 7.40; QE: 7.36
Cys^3		9.28	5.39	2.88, 2.76	
Phe^7		8.55	4.71	2.87, 2.76	QD: 6.99; QE: 7.03
DTrp^8		8.66	4.23	2.66, 2.50	HD1: 6.86; HE3: 7.49; HE1: 10.73; HZ3: 7.04; HZ2: 7.36; HH2: 7.11
IAmp^9		8.88	4.24	3.09, 2.56	QD: 7.29; QE: 7.36; QT: 4.06; HH: 8.59; QK1: 1.15; QK2: 1.15; HI: 3.15
Phe^{11}		7.72	4.90	3.19, 3.00	QD: 7.30; QE: 7.20
Cys^{14}		8.65	5.20	2.84, 2.84	
Thr^{15}		8.11	4.25	4.05	γCH_3: 1.07; OH: 5.21
NH_2		7.58,7.39			
			(B) Chemical Shifts (in ppm) of **23** in DMSO-d_6		
Cys^3	major		4.01	3.07, 2.89	
	minor				
Phe^7	major	8.87	5.03	3.01, 2.91	QD: 7.28; QE: 7.17
	minor		4.75		
DAgl^8	major	8.80	6.53		QG: 2.27; H1: 7.78; H3: 7.65; H4: 8.02; H5: 8.01; H6: 7.65; H7: 8.02; H8: 7.25
	minor	9.21	5.74		QG: 2.55; H1: 7.86; H3: 7.69; H4: 7.93; H5: 7.92; H6: 7.69; H7: 7.93; H8: 7.36
IAmp^9	major	8.24	4.27	2.92, 2.80	QD: 7.12; QE: 7.21; QT: 3.78; HH: 7.37; QK1: 1.23; QK2: 1.10; HI: 3.04
	minor				QE: 7.36; QT: 4.06; HI: 3.24
Phe^{11}	major	8.39	4.57	3.21, 2.93	QD: 7.29; QE: 7.21
	minor	8.12	4.48		
Cys^{14}	major	7.81	4.63	3.07, 2.83	
	minor	8.12	4.55		
Thr^{15}	major	7.67	4.10	4.04	γCH_3: 1.03; OH: 4.90
	minor	7.60			
NH_2		7.17, 7.29			
			(C) Chemical Shifts (in ppm) of **27** in DMSO-d_6		
Cys^3	major		3.95	3.03, 2.82	
	minor				
Phe^7	major	8.75	5.02	3.01, 2.91	QD: 7.28, QE: 7.41
	minor		4.75	3.00, 2.87	
DAgl^8	major	8.86	6.53		QG: 2.34; H1: 7.81; H3: 7.62; H4: 8.00; H5: 7.89; H6: 7.64; H7: 8.00; H8: 7.28
	minor	9.23	5.71		QG: 2.62, H5: 8.01
IAmp^9	major	8.35	4.24	2.83, 2.83	QD: 7.10; QE: 7.21; QT: 3.81; HH: 7.34; QK1: 1.23; QK2: 1.11; HI: 3.07
	minor				HH: 7.21, QT: 4.07, HI: 3.23
Tyr^{11}	major	8.30	4.41	3.08, 2.83	QD: 7.07; QE: 6.69
	minor	8.02	4.35		QD: 7.27
Cys^{14}	major	7.62	4.41	3.02, 2.80	
	minor				
NH_2	major	7.27, 7.08			

Table 3. Characterization of the NMR Structures of the Analogues Studied by NMR

parameters	**16**	**23**	**27**
restraints			
NOE distances	93	72	58
angles (deg)	23	16	7
CYANA target function	0.29	0.25	0.27
rmsd (in Å)			
backbone	0.35 ± 0.15	0.75 ± 0.18	0.12 ± 0.06
overall	1.12 ± 0.20	1.47 ± 0.31	1.92 ± 0.37
residual violations on distances			
$N_o \geq 0.1$ (Å)	0.50 ± 0.20	0.20 ± 0.06	0.40 ± 0.08
max (Å)	0.80 ± 0.15	0.06 ± 0.02	0.08 ± 0.01
dihedral angles			
$N_o \geq 1.5$, (deg)	0.0 ± 0.01	0.0 ± 0.0	0.0 ± 0.0
max (deg)	0.1 ± 0.10	0.0 ± 0.0	0.0 ± 0.0
CFF91 energies (kcal/mol)			
total energy	218 ± 9	233 ± 8	202 ± 4
van der Waals	168 ± 8	181 ± 5	174 ± 6
electrostatic	50 ± 7	51 ± 4	28 ± 2

that stabilizes the β-turn. The side chains of DPhe^2, Phe^7, and DTrp^8 are in the gauche$^+$ configuration, and the side chains of IAmp^9 and Phe^{11} are in the gauche$^-$ configuration (Table 4).

Three-Dimensional Structure of H-c[Cys^3-Phe^7-DAgl(NMe,2naphthoyl)^8-IAmp^9-Phe^{11}-Cys^{14}]-Thr^{15}-NH$_2$ (23). Analogue **23** differs from **16** by the substitution of DTrp^8 by DAgl(NMe,2naphthoyl)^8 and the deletion of DPhe^2 at the N-teminus (Table 1). With those modifications, **23** binds selectively to sst$_1$ with high affinity (IC_{50} = 1 nM). The 3D NMR structure of **23** shows that the angles around DAgl(NMe,2naphthoyl)^8 and IAmp^9 do not represent any standard β-turns (Figure 2B, Table 4). The side chains of Phe^7, DAgl(NMe,2naphthoyl)^8, IAmp^9, and Phe^{11} are in the gauche$^-$ configuration (Table 4). In addition, the side chains of Phe^7 and DAgl(NMe,2naphthoyl)^8 span a large conformational space (Figure 2B, Table 4). In the major conformer, the side chain methyl protons of DAgl(NMe,2naphthoyl)^8 give rise to NOE/ROEs to both the H1 and H8 protons of the naphthoyl group, suggesting that DAgl(NMe,2naphthoyl)^8 is in *trans* isomer in the major conformer. On the basis of the large number of NOEs

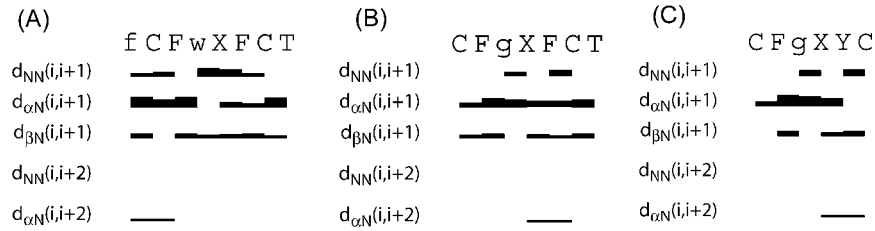

Figure 1. Survey of characteristic NOEs describing the secondary structure of analogues (A) **16**, (B) **23**, and (C) **27**. Thin, medium, and thick bars represent weak (4.5−6 Å), medium (3−4.5 Å), and strong (<3 Å) NOEs observed in the NOESY spectrum. One letter code represents the amino acids in the sequence of the peptide, where f, g, w, and X represent DPhe, DAgl(NMe, 2naphthoyl), DTrp, and IAmp, respectively.

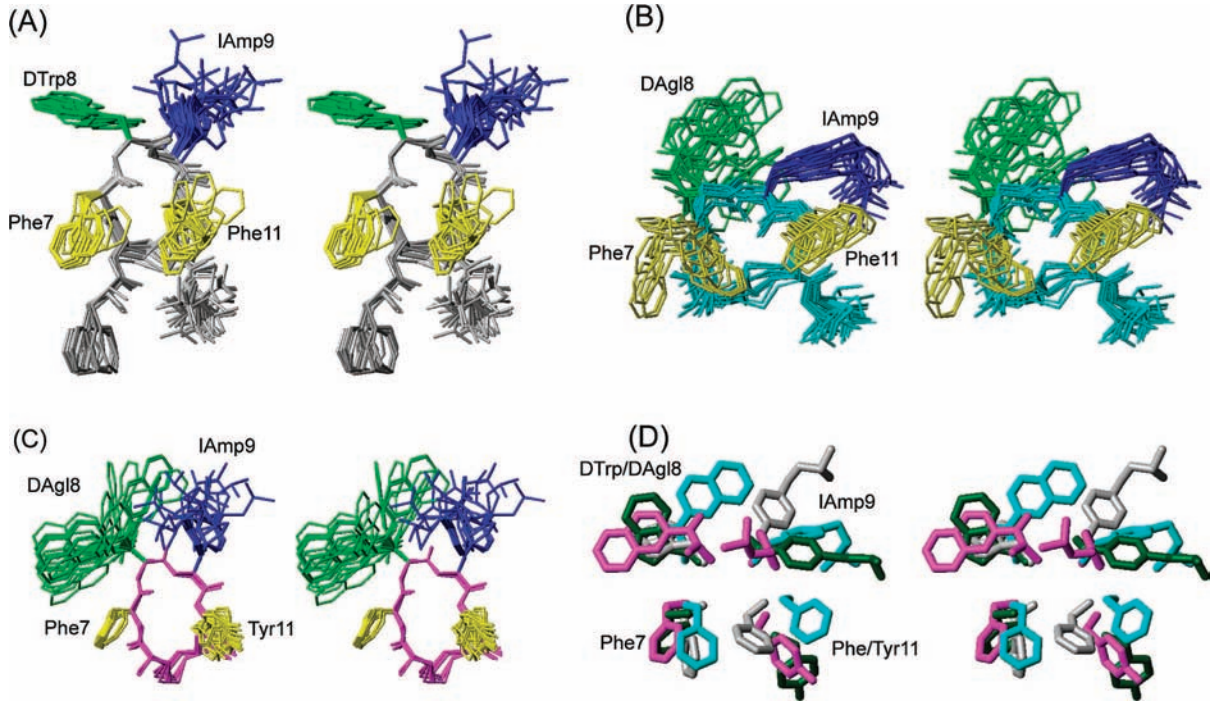

Figure 2. 3D NMR structures of analogues (A) H-DPhe-c[Cys-Phe-DTrp-IAmp-Phe-Cys]-Thr-NH_2 (**16**), (B) H-c[Cys-Phe-DAgl(NMe,2naphthoyl)-IAmp-Phe-Cys]-Thr-NH_2 (**23**), and (C) H-c[Cys-Phe-DAgl(NMe,2naphthoyl)-IAmp-Tyr-Cys]-NH_2 (**27**). For each analogue, 20 energy-minimized conformers with the lowest target function are used to represent the 3D NMR structure. The bundle is obtained by overlapping the C^{α} atoms of all the residues. The backbone and the side chains are displayed, including the disulfide bridge. The amino acid side chains that are proposed to be involved in sst$_1$ binding are highlighted: light green, DTrp/DAgl at position 8; blue, IAmp at position 9; yellow, Phe at positions 7 and 11. In (D), the side chains of sst$_1$ binding analogue **5** (in dark green) are superimposed on the structure of **16** (in gray), **23** (in cyan), and **27** (in magenta). It should be noted that the aromatic side chains at positions 7 and 11 of analogue **5** are in the other side of the peptide backbone compared to **16**, **23**, and **27**.

observed, the 3D NMR structure of the major conformer was calculated and this is assumed to be the bioactive conformation.

Three-Dimensional Structure of H-c[Cys^3-Phe^7-DAgl(NMe,2naphthoyl)^8-IAmp^9-Tyr^{11}-Cys^{14}]-NH_2 (27). The composition of **27** is different from that of **23**, with Tyr^{11} replacing Phe^{11} and the deletion of Thr^{15} at the C-terminus (Table 1), yet it binds selectively to sst$_1$ with high affinity (IC_{50} = 6 nM). The 3D NMR structure shows that the angles around DAgl(NMe,2naphthoyl)^8 and IAmp^9 do not represent any standard β-turns (Figure 2C, Table 4). The side chains of Phe^7 and Tyr^{11} are in the *gauche*$^+$ configuration, and the side chains of DAgl(NMe,2naphthoyl)^8 and IAmp^9 are in the *gauche*$^-$ configuration (Table 4). The side chains of DAgl(NMe,2naphthoyl)^8 and IAmp^9 span a large conformational space (Figure 2C, Table 4). In the major conformer, the side chain methyl protons of DAgl(NMe,2naphthoyl)^8 give rise to NOE/ROEs to both the H1 and H8 protons of the naphthoyl group, suggesting that DAgl(NMe,2naphthoyl)^8 is in *trans* isomer in the major conformer. On the basis of the large number of NOEs observed, the 3D NMR structure of the major conformer was calculated and this is assumed to be the bioactive conformation. Moreover, the minor conformer was poorly defined due to the few number of NOEs that could be identified for this conformation.

Biological Testing. To determine their SRIF receptor-binding properties, the compounds were tested for their ability to bind to cryostat sections of a membrane pellet of cells expressing the five human SRIF receptor subtypes (Table 1). For each of the tested compounds, complete competition experiments were carried out with the universal SRIF radioligand [Leu^8,-DTrp^{22},^{125}ITyr^{25}]SRIF-28(^{125}I-[LTT]-SRIF-28).[55] The results are shown in Table 1. The most potent and selective analogues were functionally evaluated for their agonist/antagonist properties using a reporter gene assay that determines the biological activity of the human sst$_1$ receptor in CCL39-sst$_1$-Luci cells, constitutively expressing the human sst$_1$ receptor as well as the luciferase gene under the control of the serum response element (SRE). The SRE is regulated by transcription factors and is activated by many extracellular signals including ligands acting at G-protein-coupled receptors.[56,57] It has been shown that upon

Table 4. Torsion Angles ϕ, Ψ, and χ_1 (in deg) of the Bundle of 20 Energy Minimized Conformers

analogue	angle	DPhe[2]	Cys[3]	Phe[7]	DTrp[8]	IAmp[9]	Phe[11]	Cys[14]	Thr[15]
16	ϕ		-174 ± 5	-108 ± 12	60 ± 7	63 ± 1	-68 ± 11	52 ± 34	-54 ± 75
	Ψ	-147 ± 1	46 ± 2	145 ± 5	31 ± 4	14 ± 2	-68 ± 24	100 ± 18	134 ± 47
	χ_1	9 ± 30	-125 ± 11	1 ± 32	27 ± 31	-109 ± 1	-168 ± 19	-100 ± 37	102 ± 76

analogue	angle	DPhe[2]	Cys[3]	Phe[7]	DAgl[8]	IAmp[9]	Phe[11]	Cys[14]	Thr[15]
23	ϕ			-84 ± 62	-13 ± 62	-117 ± 33	48 ± 7	-96 ± 26	146 ± 64
	Ψ		179 ± 60	170 ± 10	-74 ± 13	-158 ± 11	26 ± 2	-172 ± 2	-98 ± 81
	χ_1		99 ± 61	-41 ± 50	-59 ± 93	-150 ± 6	-155 ± 4	-102 ± 12	-137 ± 40

analogue	angle	DPhe[2]	Cys[3]	Phe[7]	DAgl[8]	IAmp[9]	Tyr[11]	Cys[14]	Thr[15]
27	ϕ			-156 ± 8	95 ± 4	166 ± 3	-110 ± 8	-57 ± 6	
	Ψ		132 ± 9	157 ± 1	-54 ± 1	42 ± 1	-35 ± 3	-85 ± 0	
	χ_1		34 ± 13	27 ± 1	-112 ± 102	-18 ± 80	141 ± 9	-109 ± 0	

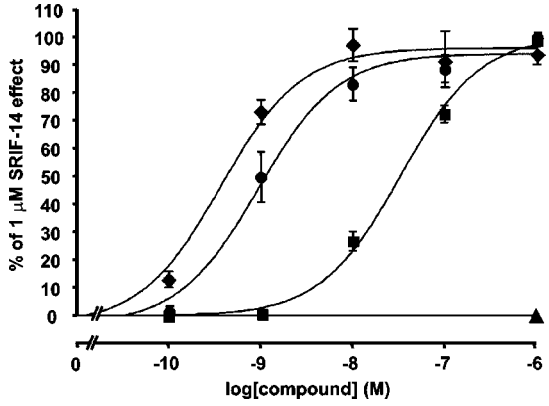

Figure 3. SRIF analogue **25** is a potent sst_1 agonist when tested in the luciferase reporter gene assay. The assay was performed as described in Experimental Procedures. CCL39-sst_1-Luci cells were treated with increasing concentrations (0.1 nmol/L, 1 nmol/L, 10 nmol/L, 100 nmol/L, and 1 μmol/mL) of SRIF (●), **33** (■), or **25** (◆). The stimulation of the luciferase reporter gene activity by the compounds is expressed as % stimulation of the 1 μmol/mL SRIF effect. Shown are the dose−response curves of the compounds. The sst_3-antagonist **35** (▲), used as negative control at 1 μmol/mL, shows no effect in the luciferase reporter gene assay.

agonist binding, SRIF receptors mediate an increase of luciferase expression via SRE in this reporter gene assay.[32,58] Figure 3 shows that stimulating CCL39-sst_1-Luci cells with somatostatin analogues activates the luciferase gene in a concentration-dependent manner. SRIF, **23**, and **25** exhibit EC_{50} values of 0.93, 3.9, and 0.37 nM, respectively, while the sst_1- agonist des-AA[1,5]-[Tyr[2],DTrp[8],IAmp[9]]-SRIF (CH-288) (**33**)[37] exhibits an EC_{50} value of 33 nM. Des-AA[1,2,4,5,12,13][DCys[3],Tyr[7],-DAgl[8](NMe,2naphthoyl)]-Cbm-SRIF(Sst$_3$-ODN-8) (**35**),[43] a short-sized somatostatin analogue with no affinity to sst_1 receptor used as a negative control, was unable to stimulate luciferase gene expression in CCL39-sst_1-Luci cells. The results of the reporter gene assay are summarized in Table 1.

Structure−Activity Relationship Studies. The proposed sst_1 receptor pharmacophore[1] derived from the NMR structures of the family of the undecamers (mono and dicyclic)[37,38] compared with the previously proposed sst_2, $sst_{2,5}$, and sst_4 pharmacophores are shown in Figure 4.

With a well-defined pharmacophore, we were now in a position to design improved analogues following a rational approach. In this regard, we designed putative sst_1-selective octa-, hepta-, and hexamers derived from the known undecamers.[1] Figure 4A shows that the sst_1-selective agonist-pharmacophore has two aromatic side chains, at position 6 or 7 and 11, in addition to the DTrp[8] and IAmp[9] pair. The sst_1 selectivity is achieved mainly through the amino acid IAmp at position 9, which replaces Lys, present in most of the somatostatin analogues. The side chain of IAmp is longer than the side chain of Lys, it has an aromatic group (amino-methylphenylalanine) extended by a relatively bulky aliphatic group (isopropyl). Hence, we conclude that IAmp cannot be accommodated in a smaller binding pocket that will fit a smaller side chain as that of Lys[9] critical for sst_{2-5} binding. We propose that only in the sst_1 receptor structure is the binding pocket large enough to accommodate the side chain of IAmp (comparing the residues in the models of the transmembrane regions of the somatostatin receptors based on the crystal structure of rhodopsin) and therefore analogues with IAmp at position 9 show selectivity for sst_1.

We wanted to identify smaller peptidic molecules than the undecamers, which would retain selectivity as well as good affinity at sst_1 receptors and possibly would act as antagonists having greater metabolic stability than the previously published analogues.[36–39,59] As we published earlier, the hypothesis that IAmp[9] by itself might establish sst_1 selectivity in the otherwise potent pan-somatostatin octapeptide des-AA[1,2,4,5,12,13]-[DTrp[8]]-SRIF (ODT-8) (**8**)[50] failed (Table 1). Substitution of Lys[9] in **8** by IAmp[9] resulted in des-AA[1,2,4,5,12,13]-[DTrp[8], IAmp[9]]-SRIF (**9**), which showed no binding affinity to any SRIF receptor,[37] most probably due to steric effects perturbing the alignment of the DTrp[8]-IAmp[9] side chains with respect to the other aromatic side chains.

Because the backbone conformations of the sst_1-selective analogues have a hairpin-like structure similar to that of the $sst_{2/3/5}$-selective octreotide-based analogues, we decided to introduce IAmp at position 9 in the octreotide scaffold with the additional substitutions (an aromatic side chain at positions 6 or 7 and at position 11) indispensable to fulfill the sst_1 pharmacophore's requirements (see below).

With the aim of searching for sst_1-selective antagonists, we first substituted Lys[9] with IAmp[9] in the published sst_2-antagonist des-AA[1,4−6,11−13]-[Cpa[2],DCys[3],Tyr[7],DTrp[8]]-SRIF-2Nal-NH_2 (**12**),[60,61] which resulted in (des-AA[1,4−6,11−13]-[Cpa[2],DCys[3],-Tyr[7],DTrp[8],IAmp[9]]-SRIF-2Nal-NH_2 (**13**) with no binding affinity to $sst_{1/4/5}$ and low binding affinity to $sst_{2/3}$ (ca. 350 nM). On the basis of the sst_1 pharmacophore, it was expected that the introduction of IAmp alone would not be sufficient for sst_1 binding (Table 1) because **13** does not have two of the aromatic residues at positions 6 or 7 and 11 necessary for sst_1 binding. Although there is an aromatic residue at position 7 in octreotide-

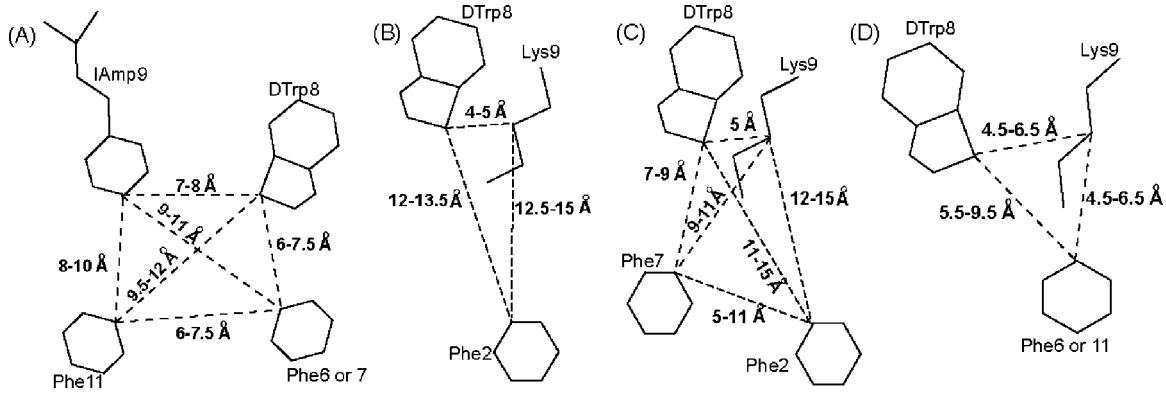

Figure 4. Schematic drawings of agonist pharmacophores for receptor-selective analogues binding to the somatostatin receptors: (A) sst$_1$, (B) sst$_2$, (C) sst$_{2/5}$, and (D) sst$_4$. The amino acid side chains, which are part of the pharmacophores, and the range of distances between the corresponding C_γ atoms of the side chains are shown.

based analogues, they do not have Phe at position 11. Hence, we replaced Thr at position 10 by Phe at 11 (as in SRIF), leaving four residues and the two Cys residues in the cycle. This analogue (**16**) exhibited similar affinity to sst$_1$ (IC_{50} = ~30 nM) as **8**, but it is more selective because it shows low affinity to the other four receptors (see Table 1). Therefore analogue **16** was selected as lead for further derivatization.

Our SAR studies focused on positions 2, 3, 8, 9, 11, and 15 of the analogue **16** (SRIF numbering). Affinities to the five SRIF receptors were determined in receptor binding assay and are summarized in Table 1.

SAR at position 2 where DPhe, Cpa, Tyr, and DTyr were substituted show that these residues can be eliminated with only small differences in binding affinity to sst$_1$ (des-AA$^{1,2,4-6,10,12,13}$-[DTrp^8,IAmp^9]-SRIF-Thr-NH$_2$ (**15**) versus **16**, des-AA$^{1,2,4-6,10,12,13}$-[DTrp^8,IAmp^9,ITyr^{11}]-SRIF-Thr-NH$_2$ (**17**) versus des-AA$^{1,4-6,10,12,13}$-[DPhe^2,DTrp^8,IAmp^9,ITyr^{11}]-SRIF-Thr-NH$_2$ (**18**), des-AA$^{1,2,4-6,10,12,13}$-[DCys^3,DTrp^8,IAmp^9,ITyr^{11}]-SRIF-2Nal-NH$_2$ (**19**) versus des-AA$^{1,4-6,10,12,13}$-[Cpa^2,DCys^3,DTrp^8,IAmp^9,ITyr^{11}]-SRIF-2Nal-NH$_2$ (**20**), des-AA$^{1,2,4-6,10,12,13}$-[LAgl(NMe,2naphthoyl)^8,IAmp^9]-SRIF-Thr-NH$_2$ (**24**) versus des-AA$^{1,4-6,10,12,13}$-[DTyr^2,LAgl(NMe,2naphthoyl)^8,IAmp^9]-SRIF-Thr-NH$_2$ (**26**), and des-AA$^{1,2,4-6,10,12,13}$-[DCys^3,DAgl(NMe,2naphthoyl)^8,IAmp^9]-SRIF-2Nal-NH$_2$ (**29**) versus des-AA$^{1,4-6,10,12,13}$-[Tyr^2,DCys^3,DAgl(NMe,2naphthoyl)^8,IAmp^9]-SRIF-2Nal-NH$_2$ (**31**)). We suggest that the individual nature of these amino acids (despite the fact that their side chains are not involved in binding) is responsible for the differences in affinity. SAR at position 3 suggests that the substitution of Cys with DCys has little effect on sst$_1$ binding affinity and function. SAR at position 8 shows the unique nature of Agl^8-containing analogues that are all highly selective for sst$_1$ over the other four receptor subtypes (**23**, **25**, **27**, **29**). Interestingly, for this scaffold, a D-configuration is significantly more favorable than the L-conformation. SAR at position 9 shows that the introduction of IAmp results in more active and selective analogues (des-AA$^{1,4-6,10,12,13}$-[Cpa^2,DCys^3,DAgl(NMe,2naphthoyl)^8]-SRIF-2Nal-NH$_2$ (**21**) versus **31**). SAR at position 11 shows that the substitution of Phe as in **15** or **16** with I-Tyr results in some loss in sst$_1$ binding affinity (**17** and **18**). SAR at position 15 shows that this residue can also be eliminated from some structures without loss of binding affinity and selectivity as in **27**. This deletion along with other most favorable substitutions yielded the hexapeptide H-c[Cys^3-Phe^7-DAgl(NMe,2naphthoyl)^8-IAmp^9-Tyr^{11}-Cys^{14}]-NH$_2$ (**27**). This peptide selectively binds to sst$_1$ with an average IC_{50} = 6.0 nM, (IC_{50} >1000 nM at sst$_2$, 317 nM at sst$_3$, 481 nM at sst$_4$, and >1000 nM at sst$_5$, respectively). Compared to our previously published analogues, which contained 11 residues, **27**, containing only 6 residues, is a much smaller and appealing molecule.

Although des-AA$^{1,4-6,12,13}$-[Tyr^2,DTrp^8,IAmp^9]-SRIF-Thr-NH$_2$ (**14**), **15**, and **17**−**20** (Table 1) showed IC_{50} for sst$_1$ in the 500 nM range, their binding affinities are significantly lower compared to that of SRIF-28 (IC_{50} for sst$_1$ = 2.9 nM), **8** (IC_{50} for sst$_1$ = 27 nM), and **5** (IC_{50} for sst$_1$ = 2.5 nM).[1] The lower affinities of these analogues could be explained based on the knowledge of the sst$_1$ pharmacophore and be due to one or more of the following reasons: (1) the distances between the side chains of the residues involved in binding may be slightly different from the distances required by the sst$_1$ pharmacophore (the distances reported for efficient receptor−ligand interactions are as follows: between DTrp^8 and IAmp^9 is 7−8 Å, between DTrp^8 and Phe$^{6/7}$ is 6−7.5 Å, between DTrp^8 and Phe^{11} is 9.5−12 Å, between IAmp^9 and Phe$^{6/7}$ is 9−11 Å, between IAmp^9 and Phe^{11} is 8−10 Å, and between Phe$^{6/7}$ and Phe^{11} is 6−7.5 Å, (Figure 4A)[1]) that the side chains possibly occupy the binding pocket partially, (2) the conformational rigidity in the side chain of DTrp at position 8 is in such a way that it cannot occupy completely the available binding pocket, (3) although the analogues have two aromatic residues, the aromatic side chains could be on the front side of the peptide backbone (when displayed from N to the C-terminus), resulting in μM binding affinity.

In the octreotide pharmacophore, the side chains of DTrp^8 and Lys^9 are in close proximity (4−6 Å),[62,63] (Figure 4C), whereas in the sst$_1$-pharmacophore, the side chains of DTrp^8 and IAmp^9 are farther apart (7−8 Å) (Figure 4A). Because the side chain of aminoglycine (Agl) has been shown to span a larger volume than the DTrp side chain, we introduced acylated Agl at position 8.[52] This substitution in the shortened analogues (**21**, **23**, **25**, **27**, **29**, and **31**) improved the binding affinity and selectivity for sst$_1$ as well. Some of these analogues also exhibit binding to sst$_4$. The introduction of Phe^{11} (**21**, **23**, **25**, **29**, and **31**) results in an aromatic group close to Lys^9/IAmp^9 as well as DTrp/DAgl^8, which satisfies the sst$_4$ pharmacophore partially and allows binding (Figure 4D, Table 5).

Following up on the observation by Bass et al.[64,65] and Hocart et al.[61] that one could turn an octreotide-based sst$_2$ agonist scaffold characterized by a DAaa^2-LCys^3 to an antagonist scaffold characterized by a LAaa^2-DCys^3, we tested **31** for agonism/antagonism. In our functional luciferase reporter gene assay, **31** along with **23**, **25**, **27**, and **29**, were agonists at human sst$_1$ (Table 1). The best analogue in this series is **25**, with an EC_{50} value of 0.37 nM in the luciferase reporter gene assay, with a binding IC_{50} of 0.19 nM, and 5000-fold selectivity versus

Table 5. Distances between C_γ Atoms (in Å) of Selected Residues for the Analogues Studied by NMR and the sst_1/sst_4 Pharmacophores[a]

	F^7-X^8	F^7-IAmp^9	F^7-F^{11}	X^8-IAmp^9	X^8-F^{11}	$IAmp^9-F^{11}$
Sst_1pharmacophore	6.0−7.5	9.0−11.0	6.0−7.5	7.0−8.0	9.5−12.0	8.0−10.0
Sst_4pharmacophore				4.5−6.5	5.5−9.5	4.5−6.5
16	5.9−7.0	9.4−9.8	5.1−6.8	5.3−6.7	8.2−8.8	8.0−8.6
23	5.9−7.8	7.3−10.6	6.6−11.0	6.9−8.1	9.6−11.2	5.8−6.6
27	5.2−6.8	8.5−10.0	6.4−7.7	4.5−7.1	9.0−9.8	6.4−8.3

[a] X refers to either DTrp or DAgl(NMe, 2naphthoyl) residues.

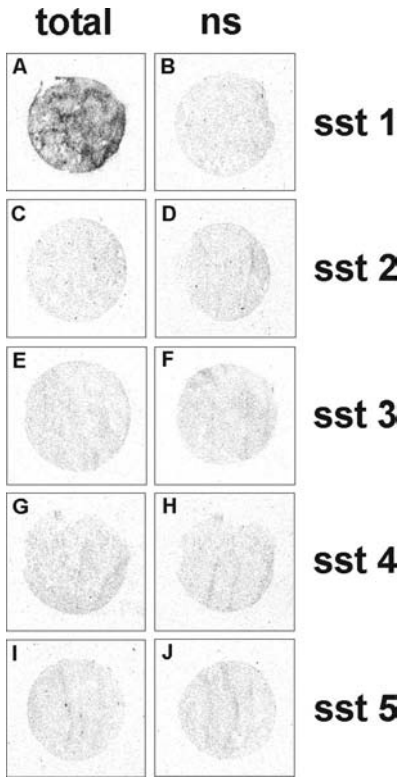

Figure 5. ^{125}I-**25** specifically labels the sst_1 expressing cell line. Autoradiograms showing total binding of ^{125}I-**25** in sst_1 (A), sst_2 (C), sst_3 (E), sst_4 (G), and sst_5 (I) receptor expressing cells. Only sst_1 cells are labeled. Autoradiograms showing nonspecific binding of ^{125}I-**25** in sst_1 (B), sst_2 (D), sst_3 (F), sst_4 (H), and sst_5 (J) receptor expressing cells (in the presence of an excess of unlabeled **25**).

$sst_{2/5}$, 500-fold selectivity versus sst_3, and 100-fold selectivity versus sst_4, respectively. SRIF and the sst_1-agonist **33** exhibit EC_{50} values of 0.93 and 33 nM, respectively. Figure 3 shows that SRIF, **25** and **33** are agonists because they effectively stimulate luciferase expression in the reporter gene assay. It is noteworthy to mention that **25** is more potent than SRIF (EC_{50}: 0.37 nM versus EC_{50}: 0.93 nM), whereas the standard sst_1 agonist **33** is approximately 100-fold less potent than either of them. We have used **35**,[3,4] a short-sized somatostatin analogue with no affinity to sst_1 receptors, as a negative control, in this test; it was found to be inactive at a concentration of 1 μM.

Analogue **25** was radio-iodinated with ^{125}I and found to bind to sections of membrane pellet of sst_1-expressing transfected cells with high specificity, as shown in Figure 5. Moreover, we evaluated the ability of the ^{125}I-**25** to bind to sst_1-expressing human cancers. Table 6 shows that this radioligand was able to label virtually all tested sst_1-expressing tumors, including a selection of well characterized sst_1-expressing prostate cancers, mesenchymal cancers, bronchial carcinoids, and gastroenteropancreatic tumors. Figure 6 and Table 6 show that compared to the strong ^{125}I-[LTT]-SRIF-28 labeling, found to be fully displaceable by **33** in these tissues and therefore indicative of sst_1 expression, the ^{125}I-**25** labeling was noticeably weaker when performed on adjacent sections of sst_1-expressing human prostate cancer. The relatively weak ^{125}I-**25**-labeling is difficult to explain because the binding affinity of the cold iodinated compound des-$AA^{1,4-6,10,12,13}$-[$D^{nat}ITyr^2$,DAgl(NMe,2naphthoyl)^8,$IAmp^9$]-SRIF-Thr-NH_2 (**34**) is in the low nanomolar range ($IC_{50} \cong 1.0$ nM for **34**). sst_2-expressing tumors, used as negative controls, were completely negative for ^{125}I-**25** binding (Table 6) despite an extremely high density of sst_2 receptors in these tumors. This further indicates the high sst_1 specificity of the tracer.

The sst_1 pharmacophore reported previously by our group showed that the side chains of four different residues are important for the binding of these analogues.[1] They are the indole ring of DTrp at position 8, IAmp side chain at position 9, and two aromatic side chains at positions 6 or 7 and 11. The distances between the side chains of these residues should be close to the values given in Table 5.[1] In addition, the sst_1 pharmacophore was different from the other SRIF receptor pharmacophores[63,66,67] in the positioning of the aromatic side chains. In all of the other SRIF receptor pharmacophores, the aromatic side chains are present at the front side of the peptide backbone when the structure of the peptide is oriented from N- to C-terminus. In contrast, in the sst_1 pharmacophore, both of the aromatic side chains are present at the back side of the peptide backbone.[1] Therefore, any peptide that has the sst_1 pharmacophore that involves the four residues at the proposed distance should bind to sst_1.

To verify the identity of the sst_1 pharmacophore, the 3D structures of three analogues, **16**, **23**, and **27**, that bind selectively to sst_1 with nM affinity were studied. All these analogues have IAmp at position 9, which is crucial for selectivity to sst_1. As shown in Figure 2, the other residues important for sst_1 binding, namely DTrp/DAgl,[8] Phe^7 and Phe/Tyr^{11}, are present in all of the three analogues. The distances between the corresponding $C\gamma$ atoms of the side chains of the four residues are given in Table 5. Comparing the distances with the sst_1 pharmacophore suggests that all of the three analogues have the sst_1 pharmacophore, except for a small discrepancy, but a detailed comparison of the structures show that the positioning of the side chains of the aromatic groups at position 7 and 11 is not exactly identical to that described for the sst_1 pharmacophore.[1] In the structures of the three analogues studied here, the aromatic side chains are present in the front side of the peptide backbone (Figure 2). Because these peptides have high binding affinity for sst_1, the binding of these peptides to sst_1 could be due to the inherent flexibility observed in these peptides. The presence of DAgl at position 8 introduces a large flexibility to the peptide backbone and in turn to the side chains of **23** and **27**, compared to **16**, which has DTrp at position 8. This is also reflected in the number of NOEs observed for **23** and **27**, which is less compared to the number of NOEs observed for **16** (Table 3). In addition, the chemical shift values observed for the aromatic protons of Phe^7 and Phe^{11} are very similar for **23** and **27** (parts B and C of Table 2), indicating a random coil or less structured elements compared to **16** (part A of Table 2). Comparing the chemical shift dispersion of the aromatic region of similar sst_2-selective octreotide-type SRIF analogues[63] with these sst_1-

Table 6. ^{125}I-**25** Specifically Labels sst$_1$-Expressing Human Cancers[a]

		^{125}I-[LTT]-SRIF-28 binding displaceable by **33**		^{125}I-**25** binding displaceable by **33**	
tumor type	no. of cases	incidence	density	incidence	density
A: sst$_1$-expressing tumors					
prostate cancer	8	8/8	+++	7/8	+
mesenchymal tumors	7	7/7	++/+++	6/7	++
bronchial carcinoids	6	6/6	++	6/6	+/++
gastroenteropancreatic tumors	4	4/4	++	4/4	+/++
B: sst$_2$-expressing tumors	8	0/8[b]	−	0/8	−

[a] +++, ++, + means high, moderate, or low receptor density, respectively. [b] ^{125}I-[LTT]-SRIF-28-binding in these tumors is fully displaceable by octreotide.

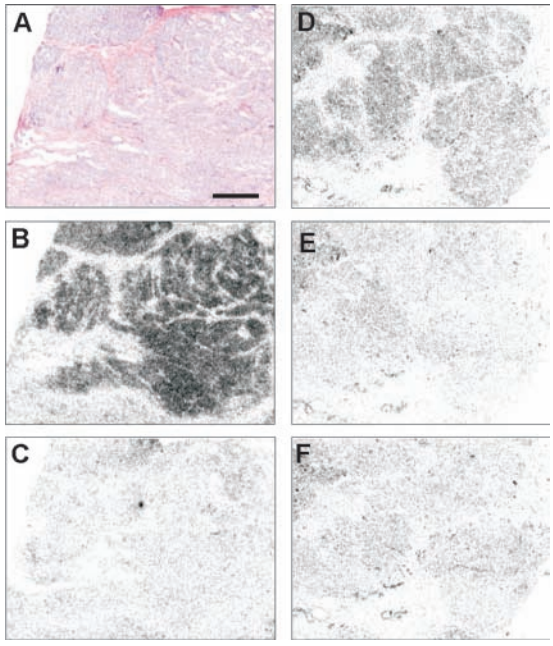

Figure 6. ^{125}I-**25** labels an sst$_1$ receptor expressing human prostate cancer. (A) Hematoxylin eosin stained tumor section (bar: 1 mm). (B,C) Autoradiograms showing total binding of ^{125}I-[LTT]-SRIF-28 with strong tumor labeling (B) that is displaceable by the sst$_1$-selective **33** (C), indicating sst$_1$ expression. (D,E,F) Autoradiograms showing total binding of ^{125}I-**25** with clear tumor labeling (D) that is displaceable by an excess of unlabeled **25** (E) or **33** (F).

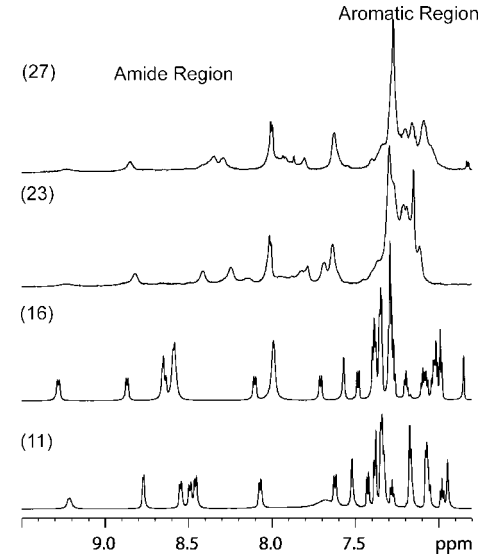

Figure 7. Amide and aromatic region of the 1D proton NMR spectra of analogues des-AA$^{1,4-6,11-13}$-[DPhe^2,DTrp^8]-SRIF-Thr-NH$_2$ (octreotide amide) (**11**), **16**, **23**, and **27**. The chemical shift dispersion of the aromatic region of analogues **11** and **16** are comparable, while those of **23** and **27** suggest that these peptides are less structured in DMSO compared to analogues **11** and **16**.

selective analogues suggests that the latter are less structured in DMSO (Figure 7). On the basis of the conformational flexibility of **23** and **27** (parts B and C of Table 2, it is suggested that the aromatic side chains could move to the backside of the peptide backbone for sst$_1$ binding. The higher binding affinity of **23** and **27** compared to that of **16** could be due to the larger flexibility of the peptide backbone of the former, resulting in a better fit of **23** and **27** into the sst$_1$ binding pocket compared to **16**, which shows a single conformation with much less flexibility for its peptide backbone (parts A−D of Figure 2, Table 5).

Conclusions

To conclude, using a pharmacophore derived from the structures of undecamers,[1] we were able to design somatostatin heptamers and hexamers with improved or similar affinity and sst$_1$ selectivity compared to the previously published undecamers. Although the positioning of the aromatic side chains in these shortened analogues is not exactly identical to that found for the sst$_1$ pharmacophore proposed earlier, backbone flexibility is suggested as a mechanism for induced fit necessary for sst$_1$ binding.

These results demonstrate that rational and efficient SAR in peptides is possible. In this case, it was critical that the structure of the original pharmacophore be well-defined and accurate. This was the case because it was based on the structures of several high affinity ligands of differing primary sequences.[1] The most potent of these sst$_1$-selective analogues (**25**) in respect of affinity, selectivity, and functionality could be radio-iodinated. While this tracer is highly specific for labeling sst$_1$-expressing tumors with very high binding affinity, the sensitivity of the assay using this radioligand remains below expectations. This is somewhat disappointing, but it should be kept in mind that agonist radioligands are not devoid of caveats. We have shown previously that although ^{125}I-[LTT]-SRIF-28, [^{125}I]Tyr^{10}-CST$_{14}$, or [^{125}I]Tyr^3-octreotide are excellent radioligands showing high affinity and high specific binding in studies using membranes of recombinantly expressed SRIF receptors in CCL-39 or other cells,[68,69] it is clear that [^{125}I]Tyr^{10}-CST$_{14}$ is by far inferior as a radioligand compared to ^{125}I-[LTT]-SRIF-28 or [^{125}I]Tyr^3-octreotide in receptor autoradiography when using slices of brain or peripheral tissues known to express SRIF receptors,[70] illustrating the fact that all agonists are not equal.

Experimental Procedures

Chemistry: Starting Materials. The Boc-Cys(Mob)-CM resin with a capacity of 0.3−0.5 mequiv/g was obtained according to published procedures.[71] All N^{α}-*tert*-butoxycarbonyl (BOC) protected amino acids with side chain protection were purchased from Bachem Inc. (Torrance, CA), Chem-Impex International (Wood Dale, IL), Novabiochem (San Diego, CA), or Reanal (Budapest, Hungary). The side chain protecting groups were as follows: Cys(Mob), Lys[Z(2Cl)] Ser(Bzl), Thr(Bzl), Tyr[Z(2Br)], and *m*-I-Tyr[Bzl(3Br)]. Boc-IAmp(Z),[72] Fmoc-D/LAgl(NMe,Boc),[46] and

Fmoc-DAgl(Boc)[73] were synthesized in our laboratory. All reagents and solvents were reagent grade or better and used without further purification.

Peptide Synthesis. Peptides were synthesized by the solid-phase approach with Boc chemistry either manually or on a CS-Bio peptide synthesizer model CS536. Boc-Cys(Mob)-CM resin with a capacity of 0.3−0.5 mequiv/g or 4-methylbenzhydrylamine (MBHA) resin with a capacity of 0.4 mequiv/g was used, respectively. Couplings of the protected amino acids were mediated by diisopropylcarbodiimide (DIC) and (HOBt) in DMF for 1 h and monitored by the qualitative ninhydrin test.[74] A 3 equiv excess of the protected amino acids based on the original substitution of the resin was used in most cases. Boc removal was achieved with trifluoroacetic acid (60% in CH_2Cl_2, 1−2% ethanedithiol or *m*-cresol) for 20 min. An isopropyl alcohol (1% *m*-cresol) wash followed TFA treatment, and then successive washes with triethylamine solution (10% in CH_2Cl_2), methanol, triethylamine solution, methanol, and CH_2Cl_2 completed the neutralization sequence. D/L-Agl(NMe,2naphthoyl) residue was formed on the resin. In short: after Fmoc-D/LAgl(NMe,Boc)-OH was coupled, the Boc protecting group was removed with TFA, 3 equiv 2naphthoyl chloride, and 3 equiv DIPEA were used to acylate the free secondary amino group of the side chain. Removal of the N^{α}-Fmoc protecting group with 20% piperidine in DMF in two successive 5 and 15 min treatments was followed by the standard elongation protocol until the completion of the peptide.

All of the peptides were cleaved from the resin support with simultaneous side chain deprotection by anhydrous HF containing the scavengers anisole (10% v/v) and methyl sulfide (5% v/v) for 60 min at 0 °C. The diethyl ether precipitated crude peptides were cyclized in 75% acetic acid (200 mL) by addition of iodine (10% solution in methanol) until the appearance of a stable orange color. Forty minutes later, ascorbic acid was added to quench the excess iodine.

Purification and Characterization of the Analogues. The crude, lyophilized peptides were purified by preparative RP-HPLC[49] on a 5 cm × 30 cm cartridge, packed in the laboratory with reversed-phase Vydac C_{18} silica (15−20 μM particle size, 300 Å) using a Waters Prep LC 4000 preparative chromatograph system with a Waters 486 tunable absorbance UV detector and Huston Instruments Omni Scribe chart recorder. The peptides eluted with a flow rate of 100 mL/min using a linear gradient of 1% B per 3 min increase from the baseline % B. Eluent A = 0.25 N TEAP pH 2.25, eluent B = 60% CH_3CN, 40% A. As a final step, all peptides were rechromatographed in a 0.1% TFA solution and CH_3CN on the same cartridge at 100 mL/min (gradient of 1% CH_3CN/min). The collected fractions were screened by analytical RP-HPLC on a system using two Waters 501 HPLC pumps, a Schimadzu SPD-6A UV detector, a Rheodyne model 7125 injector, a Huston Instruments Omni Scribe chart recorder, and a Vydac C_{18} column (0.46 cm × 25 cm, 5 μm particle size, 300 Å pore size). The fractions containing the product were pooled and subjected to lyophilization. The purity of the final peptide was determined by analytical RP-HPLC performed with a linear gradient using 0.1 M TEAP pH 2.5 as eluent A and 60% CH_3CN/40% A as eluent B on a Hewlett-Packard series II 1090 liquid chromatograph connected to a Vydac C_{18} column (0.21 cm × 15 cm, 5 μm particle size, 300 Å pore size). The capillary zone electrophoresis (CZE) analysis of the peptides was performed on a Beckman P/ACE System 2050; field strength of 15 kV at 30 °C on an Agilent μSil bare fused-silica capillary (75 μm id × 40 cm length).[51] Mass spectra (MALDI-TOF-MS) were measured on an ABI-Perseptive DE-STR instrument. The instrument employs a nitrogen laser (337 nm) at a repetition rate of 20 Hz. The applied accelerating voltage was 20 kV. Spectra were recorded in delayed extraction mode (300 ns delay). All spectra were recorded in the positive reflector mode. Spectra were sums of 100 laser shots. Matrix α-cyano-4-hydroxycinnamic acid was prepared as saturated solutions in 0.3% TFA in 50% CH_3CN. The observed monoisotopic $(M + H)^+$ values of each peptide corresponded with the calculated $(M + H)^+$ values (Table 1). The diastereomers of the Agl containing peptides could be separated by preparative RP-HPLC.

Determination of the Stereochemistry of Agl in the Peptides. Because the L and D enantiomers of Fmoc-D/LAgl(NMe,Boc)[46] used for the synthesis of peptides (**21**, des-$AA^{1,4-6,10,12,13}$-[Cpa^2,$DCys^3$,LAgl(NMe,2naphthoyl)^8]-SRIF-2Nal-NH_2 (**22**), **23**−**25**, **27**, des-$AA^{1,2,4-6,10,12,13}$-[LAgl(NMe,2naphthoyl)^8, $IAmp^9$,Tyr^{11}]-SRIF-NH_2 (**28**), **29**, des-$AA^{1,2,4-6,10,12,13}$-[$DCys^3$,LAgl-(NMe,2naphthoyl)^8,$IAmp^9$]-SRIF-2Nal-NH_2 (**30**), **31**, and des-$AA^{1,4-6,10,12,13}$-[Tyr^2,$DCys^3$,LAgl(NMe,2naphthoyl)^8,$IAmp^9$]-SRIF-2Nal-NH_2 (**32**)) were not resolved initially, two diastereomers were generated, isolated, characterized, and tested. Separation of the L-from the DAgl-containing peptides was achieved using RP-HPLC. The absolute configuration of the Agl was deduced from enzymatic hydrolysis studies with trypsin, aminopeptidase M, and proteinase K (Roche Diagnostics Corp., Indianapolis, IN), respectively, as we published earlier.[50] All enzymatic hydrolyses were carried out according to the protocols suggested by the manufacturers.

Trypsin, which is highly specific toward positively charged side chains with lysine and arginine, was used to determine the stereochemistry of **21** and **22**. Trypsin (Roche, 5 μg) in 0.05% TFA (20 μL) was added to peptide (0.02 μmol) dissolved in 0.046 M Tris buffer (200 μL, pH = 8.1) containing 0.01 M $CaCl_2$. The hydrolysis was followed by RP-HPLC for 6 days. Trypsin was able to open the ring structure of **21** and **22**, but the rate of reactions was very much different. We suggest that **22** contains the L-isomer of the Agl derivative and **21** contains the D-isomer of the Agl derivative because 55% of **22** versus only 28% of **21** were hydrolyzed in 6 days.

Peptides with L-amino acids at their N-terminus and IAmp at position 9 instead of Lys (**23** versus **24** and **27** versus **28**) were digested with aminopeptidase M, which is a metalloprotease, and can hydrolyze peptides at a free α-amino group of L-amino acids (except X-Pro bonds and the amino groups of Asp, Gln, or βAla) to determine the absolute configuration of Agl. The treatment of **24** and **28** with aminopeptidase M at room temperature for 48 h resulted in many very hydrophilic products followed by RP-HPLC, indicating that these peptides have been completely hydrolyzed, providing evidence that these analogues contained the L-enantiomer of Agl in their sequence. Compounds **23** and **27** were hydrolyzed only into two products, suggesting that these two peptides contained the D-enantiomer of Agl in their sequence, resulting in more resistance to the enzymatic hydrolysis. To confirm this conclusion, these analogues were also digested with proteinase K, which is a serine protease that exhibits very broad cleavage specificity. The predominant site of cleavage is the peptide bond adjacent to the carboxyl group of hydrophobic aliphatic and aromatic amino acids with blocked α amino groups. Peptides were dissolved (20 μg) at a concentration of 0.3 mg/mL in 10 mM Tris buffer pH 7.8. Proteinase K (5 μL, 6 U) was added and reacted for 16 h at 37 °C. An aliquot (5 μL) was quenched with 45 μL 0.1 N HCl prior to analysis by HPLC for determination of degradation products. The aliquots were screened using microbore RP-HPLC under buffer system A; 0.1%TFA/H_2O, buffer system B, 70% CH_3CN in A at a flow rate of 0.05 mL/min under gradient conditions 10−80% B over 30 min. Fragments of **23** identified as H-Phe-Agl(NMe,-2naphthoyl)-IAmp-Phe-Cys-Thr-NH_2 and H-Phe-Agl(NMe,2naphthoyl)-IAmp-Phe-OH were confirmed by MALDI-MS. These observations verified that **23** contained the DAgl. The mass of fragments of **24** were found to be <500 Da, indicating the presence of LAgl.

Analogues **25**, **26**, **29**, **30**, and **31** and **32** contain a D-residue at position 2 (DTyr) or 3 (DCys), respectively, therefore enzymatic hydrolysis by aminopeptidase M could not be expected for any of these compounds. Instead, these analogues were digested with proteinase K as described above.

The digestion of **25** with proteinase K for 4 days resulted in four products, which were identified as H-cyclo[Cys-Phe-Agl(NMe,2naphthoyl)-IAmp-Phe-Cys]-Thr-NH_2, H-Phe-Agl(NMe,-2naphthoyl)-IAmp-Phe-Cys-Thr-NH_2, H-Phe-Agl(NMe,2naphthoyl)-IAmp-Phe-OH, and the starting material H-DTyr-cyclo[Cys-Phe-Agl(NMe,2naphthoyl)-IAmp-Phe-Cys]-Thr-NH_2, confirmed by MAL-

Table 7. Separation of the D- from the L-Agl-Containing Peptides by RP-HPLC[a]

compd	HPLC-column	gradient	retention time (min)
21	Vydac C_{18}	20−80%B in 40 min	32.33
22	Vydac C_{18}	20−80%B in 40 min	35.26
23	Vydac C_{18}	30− 60%B in 30 min	17.93
24	Vydac C_{18}	30−60%B in 30 min	23.39
25	Gemini C_{18}	20−60%B in 40 min	30.56
26	Gemini C_{18}	20−60%B in 40 min	34.15
27	Vydac C_{18}	30−70%B in 30 min	11.75
28	Vydac C_{18}	30−70%B in 30 min	14.91
29	Gemini C_{18}	40−70%B in 30 min	20.28
30	Gemini C_{18}	40−70%B in 30 min	25.10
31	Vydac C_{18}	30−70%B in 40 min	27.68
32	Vydac C_{18}	30−70%B in 40 min	32.75

[a] HPLC buffer system: A = TEAP (pH 2.5) and B = 60% CH_3CN/40% A with a gradient slope of 1% B/min at flow rate of 0.2 mL/min.

DI-MS. After the digestion of **26** with proteinase K for 4 days, no starting material was detected by HPLC, one of the fragments was identified as H-DTyr-Cys-Phe-Agl(NMe,2naphthoyl)-IAmp-Phe-Cys-OH and all of the other detected fragments had a mass of less than 500, suggesting that this peptide contains the L-isomer of Agl.

The digestion of **29** with proteinase K for 7 days resulted in three products, which were identified as H-cyclo[DCys-Phe-Agl(NMe,2-naphthoyl)-IAmp-Phe-Cys]-OH, H-DCys-Phe-Agl(NMe,2naphthoyl)-IAmp-Phe-OH, and the starting material H-cyclo[DCys-Phe-Agl(NMe,2naphthoyl)-IAmp-Phe-Cys]-Nal-NH_2, confirmed by MALDI-MS. After the digestion of **30** with proteinase K for 47 h, a small amount of the starting material was detected by HPLC and the fragments were identified as H-Agl(NMe,-2naphthoyl)-IAmp-Phe-OH and H-IAmp-Phe-Cys-Nal-NH_2 confirmed by MALDI-MS, suggesting that this peptide contains the L-isomer of Agl.

The digestion of **31** with proteinase K for 47 h resulted in three fragments, which were identified as H-cyclo[DCys-Phe-Agl(NMe,2naphthoyl)-IAmp-Phe-Cys]-Nal-NH_2, H-DCys-(Cys-Nal-NH_2)-Phe-Agl(NMe,2naphthoyl)-IAmp-Phe-OH, and H-DCys-Phe-Agl(NMe,2naphthoyl)-IAmp-Phe-OH and the starting material confirmed by MALDI-MS. After the digestion of **32** with proteinase K for 47 h, a small amount of the starting material was detected by HPLC and no other fragments could be identified, suggesting that this peptide contains the L-isomer of Agl.

Overall, aminoglycine-containing enantiomers were relatively easy to separate using HPLC under gradient conditions (Table 7).

NMR Experiments. The ^{1}H NMR spectra were recorded on a Bruker 700 MHz spectrometer operating at proton frequency of 700 MHz. Chemical shifts were measured using DMSO ($\delta = 2.49$ ppm) as an internal standard. The 2D spectra were acquired at 298 K. Resonance assignments of the various proton resonances have been carried out using total correlation spectroscopy (TOCSY),[75,76] double-quantum filtered spectroscopy (DQF-COSY),[77] and nuclear Overhauser enhancement spectroscopy (NOESY).[78–80] The TOCSY experiments employed the MLEV-17 spin-locking sequence suggested by Davis and Bax,[75] applied for a mixing time of 50 or 70 ms. The NOESY experiments were carried out with a mixing time of 100 or 150 ms. The TOCSY and NOESY spectra were acquired using 800 complex data points in the ω_1 dimension and 1024 complex data points in the ω_2 dimension and were subsequently zero-filled to 1024 × 2048 before Fourier transformation. The DQF-COSY spectra were acquired with 1024 × 4096 data points and were zero-filled to 2048 × 4096 before Fourier transformation. The TOCSY, DQF-COSY, and NOESY spectra were acquired with 16, 16, and 24 scans, respectively, with a relaxation delay of 1 s. The signal from the residual water of the solvent was suppressed using presaturation during the relaxation delay and during the mixing time. The TOCSY and NOESY data were multiplied by a 75° shifted sine-function in both dimensions. To differentiate exchange peaks from the NOEs, rotating frame NOESY (ROESY)[81,82] spectra were measured at 150, 250, and 400 ms. All spectra were processed using the software PROSA.[83] The spectra were analyzed using the software X-EASY.[84]

Structure Determination. The chemical shift assignment of the major/minor conformer was obtained by the standard procedure using DQF-COSY and TOCSY spectra for intraresidual assignment and the NOESY spectrum was used for the sequential assignment.[85] The collection of structural restraints is based on the NOEs and vicinal $^3J_{NH\alpha}$ couplings. Dihedral angle constraints were obtained from the $^3J_{NH\alpha}$ couplings, which were measured from the 1D ^{1}H NMR spectra and from the intraresidual and sequential NOEs along with the macro GRIDSEARCH in the program CYANA.[53] The calibration of NOE intensities versus ^{1}H−^{1}H distance restraints and appropriate pseudoatom corrections to the nonstereo specifically assigned methylene, methyl, and ring protons were performed using the program CYANA. On an average, approximately 70 NOE constraints and 15 angle constraints were utilized while calculating the conformers (Table 3). A total of 100 conformers were initially generated by CYANA, and a bundle containing 20 CYANA conformers with the lowest target function values were utilized for further restrained energy minimization using the program DISCOVER with steepest decent algorithm.[54] The resulting energy minimized bundle of 20 conformers was used as a basis for discussing the solution conformation of the different SRIF analogues. The structures were analyzed using the program MOLMOL.[86]

Biology: Reagents. All reagents were of the best grade available and were purchased from common suppliers. Lactalbumin hydrolysate was from HyClone, ATP from Sigma-Aldrich, D-luciferin from Roche Diagnostics, and coenzyme A from Calbiochem.

Cell Lines. Chinese hamster lung fibroblasts (CCL39) stably expressing the human sst$_1$ and the luciferase reporter gene under the control of the serum response element (CCL39-sst$_1$-Luci) were from D. Hoyer (Novartis, Basel, Switzerland) and grown in DMEM with GlutaMAX-I/Ham's F-12 Nut. Mix. with GlutaMAX-I (1:1) supplemented with 10% fetal bovine serum, 100U/mL penicillin, 100 μg/mL streptomycin, and 400 μg/mL geneticin (G418-sulfate) at 37 °C and 5% CO_2. All culture reagents were from Gibco BRL, Life Technologies.

Receptor Autoradiography. Cell membrane pellets were prepared as previously described and stored at −80 °C.[87] Receptor autoradiography was performed on 20 μm thick cryostat (Microm HM 500, Walldorf, Germany) sections of the membrane pellets, mounted on microscope slides, and then stored at −20 °C. For each of the tested compounds, complete competition experiments with the universal SRIF radioligand [Leu^8, D-Trp^{22}, ^{125}I-Tyr^{25}]-SRIF-28 (^{125}I-[LTT]-SRIF-28) (2000 Ci/mmol; ANAWA, Wangen, Switzerland) using 15000 cpm/100 μL and increasing concentrations of the unlabeled peptide ranging from 0.1 to 1000 nM were performed. As control, unlabeled SRIF-28 was run in parallel using the same increasing concentrations. The sections were incubated with ^{125}I-[LTT]-SRIF-28 for 2 h at room temperature in 170 mmol/L Tris-HCl buffer (pH 8.2) containing 1% BSA, 40 mg/L bacitracin, and 10 mmol/L $MgCl_2$ to inhibit endogenous proteases. The incubated sections were washed twice for 5 min in cold 170 mmol/L Tris-HCl (pH 8.2) containing 0.25% BSA. After a brief dip in 170 mmol/L Tris-HCl (pH 8.2), the sections were dried quickly and exposed for 1 week to Kodak BioMax MR film. IC_{50} values were calculated after quantification of the data using a computer-assisted image processing system as described previously.[88] Tissue standards (Autoradiographic [^{125}I] and/or [^{14}C] microscales, GE Healthcare, Little Chalfont, UK) that contain known amounts of isotope, cross-calibrated to tissue-equivalent ligand concentrations, were used for quantification.[88–91]

The analogue **25** was ^{125}I-monoradiolabeled (2000 Ci/mmol, ANAWA, Switzerland) and used as radioligand in binding studies on cell membrane pellet sections of cells stably expressing sst$_1$ receptors and on tissue sections, following the same protocol as described above for ^{125}I-[LTT]-SRIF-28.

Luciferase Assay. The luciferase reporter gene assay was performed as described previously by Hoyer and colleagues[32,58] with minor modifications. CCL39-sst$_1$-Luci cells were seeded at 25000 cells per well in 96-well plates. After 24 h, the cells were washed once with PBS and then serum-deprived for 24 h in assay

medium (DMEM with GlutaMax-I/Ham's F12 Nut. Mix. with GlutaMax-I (1:1) containing 5 g/L lactalbumin hydrolysate and 20 mM HEPES) at 37 °C and 5% CO_2. The cells were then treated in triplicate at 37 °C and 5% CO_2 with assay medium alone (basal) or with assay medium containing the compounds to be tested at concentrations between 0.1 nM and 1 μM for 5 h. The cells were then washed with PBS and lysed in lysis buffer (100 mM KPi-buffer containing 0.2% Triton X-100 and 1 mM DL-dithiothreitol). Luciferase activity was measured using a luminometer by injecting first the ATP reagent (10 mM ATP, 35 mM glycyl-glycine, and 20 mM $MgCl_2$, pH 7.8) and then the luciferin reagent (0.47 mM D-luciferin, 0.27 mM coenzyme A, 35 mM glycyl-glycine, and 20 mM $MgCl_2$, pH 7.8). Measuring parameters: delay time, 5 s; measurement time, 10 s. The 1 μM SRIF-14 effect minus the basal effect was set as 100%. Stimulation of luciferase reporter gene activity by the different compounds is expressed as % stimulation of the 1 μM SRIF-14 effect. As positive control for the luciferase reporter gene activity, 10% fetal bovine serum in assay medium was used.

Acknowledgment. The project described was supported in part by award no. 5R01DK59953-05 from the National Institute of Diabetes and Digestive and Kidney Diseases. The content is solely the responsibility of the authors and does not necessarily represent the official views of the National Institute of Diabetes and Digestive and Kidney Diseases or the National Institutes of Health. We are indebted to R. Kaiser and C. Miller for technical assistance in the synthesis and characterization of the peptides and Dr. W. Fisher, and William Low for mass spectrometric analyses. J.R. is the Dr. Frederik Paulsen Chair in Neurosciences Professor.

References

(1) Grace, C. R. R.; Durrer, L.; Koerber, S. C.; Erchegyi, J.; Reubi, J. C.; Rivier, J. E.; Riek, R. Somatostatin receptor 1 selective analogues: 4. Three-dimensional consensus structure by NMR. *J. Med. Chem.* **2005**, *48*, 523–533.

(2) Brazeau, P.; Vale, W. W.; Burgus, R.; Ling, N.; Butcher, M.; Rivier, J. E.; Guillemin, R. Hypothalamic polypeptide that inhibits the secretion of immunoreactive pituitary growth hormone. *Science* **1973**, *179*, 77–79.

(3) Guillemin, R.; Gerich, J. E. Somatostatin: physiological and clinical significance. *Ann. Rev. Med.* **1976**, *27*, 379–388.

(4) Tannenbaum, G. S.; Epelbaum, J. Somatostatin. In *Handbook of Physiology—The Endocrine System*; Kostyo, J. L., Goodman, H. M. , Eds.; Oxford University Press: New York, 1999; Vol. V: Hormonal Control of Growth, pp 221−265.

(5) Janecka, A.; Zubrzycka, M.; Janecki, T. Review: Somatostatin Analogs. *J. Pept. Res.* **2001**, *58*, 91–107.

(6) Schally, A. V.; Comaru-Schally, A. M.; Nagy, A.; Kovacs, M.; Szepeshazi, K.; Plonowski, A.; Varga, J. L.; Halmos, G. Hypothalamic hormones and cancer. *Front. Neuroendocrinol.* **2001**, *22*, 248–291.

(7) Hannon, J. P.; Nunn, C.; Stolz, B.; Bruns, C.; Weckbecker, G.; Lewis, I.; Troxler, T.; Hurth, K.; Hoyer, D. Drug design at peptide receptors: somatostatin receptor ligands. *J. Mol. Neurosci.* **2002**, *18*, 15–27.

(8) Hoyer, D.; Epelbaum, J.; Feniuk, W.; Humphrey, P. P. A.; Meyerhof, W.; O'Caroll, A. M.; Patl, Y.; Reisine, T.; Reubi, J. C.; Schindler, M.; Schonbrunn, A.; Taylor, J. E.; Vezzani, A. Somatostatin receptors. In *The IUPHAR Compendium of Receptor Characterization and Classification*, 2nd ed.; Girdlestrom, D. , Ed.; IUPHAR Media: London, 2000; pp354−364.

(9) Csaba, Z.; Dournaud, P. Cellular biology of somatostatin receptors. *Neuropeptides* **2001**, *35*, 1–23.

(10) Patel, Y. C. Somatostatin and its receptor family. *Front. Neuroendocrinol.* **1999**, *20*, 157–198.

(11) Siehler, S.; Hoyer, D. Characterisation of human recombinant somatostatin receptors. 4. Modulation of phospholipase C activity. *Naunyn-Schmiedeberg's Arch. Pharmacol.* **1999**, *360*, 522–532.

(12) Cescato, R.; Schulz, S.; Waser, B.; Eltschinger, V.; Rivier, J. E.; Wester, H.-J.; Culler, M.; Ginj, M.; Liu, Q.; Schonbrunn, A.; Reubi, J. C. Internalization of sst_2, sst_3, and sst_5 receptors: effects of somatostatin agonist and antagonists. *J. Nucl. Med.* **2006**, *47*, 502–511.

(13) Ginj, M.; Zhang, H.; Waser, B.; Cescato, R.; Wild, D.; Erchegyi, J.; Rivier, J.; Mäcke, H. R.; Reubi, J. C. Radiolabeled somatostatin receptor antagonists are preferable to agonists for in vivo peptide receptor targeting of tumors. *Proc. Natl. Acad. Sci. U.S.A.* **2006**, *103*, 16436–16441.

(14) Olias, G.; Viollet, C.; Kusserow, H.; Epelbaum, J.; Meyerhof, W. Regulation and function of somatostatin receptors. *J. Neurochem.* **2004**, *89*, 1057–1091.

(15) Weckbecker, G.; Lewis, I.; Albert, R.; Schmid, H. A.; Hoyer, D.; Bruns, C. Opportunities in somatostatin research: biological, chemical, and therapeutic aspects. *Nat. Rev. Drug Discovery* **2003**, *2*, 999–1017.

(16) Piwko, C.; Thoss, V. S.; Schupbach, E.; Kummer, J.; Langenegger, D.; Probst, A.; Hoyer, D. Pharmacological characterisation of human cerebral cortex somatostatin SRIF1 and SRIF2 receptors. *Naunyn-Schmiedeberg's Arch. Pharmacol.* **1997**, *355*, 161–167.

(17) Thermos, K. Functional mapping of somatostatin receptors in the retina: a review. *Vision Res.* **2003**, *43*, 1805–1815.

(18) Bocci, G.; Culler, M. D.; Fioravanti, A.; Orlandi, P.; Fasciani, A.; Colucci, R.; Taylor, J. E.; Sadat, D.; Danesi, R.; Del Tacca, M. In vitro antiangiogenic activity of selective somatostatin subtype-1 receptor agonists. *Eur. J. Clin. Invest.* **2007**, *37*, 700–708.

(19) Reubi, J. C.; Schaer, J. C.; Waser, B.; Hoeger, C.; Rivier, J. A selective analog for the somatostatin sst1-receptor subtype expressed by human tumors. *Eur. J. Pharmacol.* **1998**, *345*, 103–110.

(20) Reubi, J. C.; Waser, B.; Laissue, J. A.; Gebbers, J. O. Somatostatin and vasoactive intestinal peptide receptors in human mesenchymal tumors: in vitro identification. *Cancer Res.* **1996**, *56*, 1922–1931.

(21) Reubi, J. C.; Waser, B.; Schaer, J.-C.; Laissue, J. A. Somatostatin receptor sst1−sst5 expression in normal and neoplastic human tissues using receptor autoradiography with subtype-selective ligands. *Eur. J. Nucl. Med.* **2001**, *28*, 836–846.

(22) Reubi, J. C.; Schaer, J. C.; Waser, B.; Mengod, G. Expression and localization of somatostatin receptor SSTR1, SSTR2, and SSTR3 mRNAs in primary human tumors using in situ hybridization. *Cancer Res.* **1994**, *54*, 3455–3459.

(23) Reubi, J. C.; Waser, B.; Schaer, J. C.; Markwalder, R. Somatostatin receptors in human prostate and prostate cancer. *J. Clin. Endocrinol. Metab.* **1995**, *80*, 2806–2814.

(24) Miller, G. M.; Alexander, J. M.; Bikkal, H. A.; Katznelson, L.; Zervas, N. T.; Klibanski, A. Somatostatin receptor subtype gene expression in pituitary adenomas. *J. Clin. Endocrinol. Metab.* **1995**, *80*, 1386–1392.

(25) Lanneau, C.; Bluet-Pajot, M. T.; Zizzari, P.; Csaba, Z.; Dournaud, P.; Helboe, L.; Hoyer, D.; Pellegrini, E.; Tannenbaum, G. S.; Epelbaum, J.; Gardette, R. Involvement of the sst1 somatostatin receptor subtype in the intrahypothalamic neuronal network regulating growth hormone secretion: an in vitro and in vivo antisense study. *Endocrinology* **2000**, *141*, 967–979.

(26) Kreienkamp, H.-J.; Akgün, E.; Baumeister, H.; Meyerhof, W.; Richter, D. Somatostatin receptor subtype 1 modulates basal inhibition of growth hormone release in somatotrophs. *FEBS Lett.* **1999**, *462*, 464–466.

(27) Zatelli, M. C.; Piccin, D.; Tagliati, F.; Ambrosio, M. R.; Margutti, A.; Padovani, R.; Scanarini, M.; Culler, M. D.; degli Uberti, E. C. Somatostatin receptor subtype 1 selective activation in human growth hormone (GH)- and prolactin (PRL)-secreting pituitary adenomas: effects on cell viability, GH, and PRL secretion. *J. Clin. Endocrinol. Metab.* **2003**, *88*, 2797–2802.

(28) Vasilaki, A.; Papasava, D.; Hoyer, D.; Thermos, K. The somatostatin receptor (sst(1)) modulates the release of somatostatin in the nucleus accumbens of the rat. *Neuropharmacology* **2004**, *47*, 612–618.

(29) Dal Monte, M. D.; Petrucci, C.; Vasilaki, A.; Cervia, D.; Grouselle, D.; Epelbaum, J.; Kreienkamp, H. J.; Richter, D.; Hoyer, D.; Bagnoli, P. Genetic deletion of somatostatin receptor 1 alters somatostatinergic transmission in the mouse retina. *Neuropharmacology* **2003**, *45*, 1080–1092.

(30) Thermos, K.; Bagnoli, P.; Epelbaum, J.; Hoyer, D. The somatostatin sst1 receptor: an autoreceptor for somatostatin in brain and retina. *Pharmacol. Ther.* **2006**, *110*, 455–464.

(31) Hoyer, D.; Dixon, K.; Gentsch, C.; Vassout, A.; Enz, A.; Jaton, A.; Nunn, C.; Schoeffter, P.; Neumann, P.; Troxler, T.; Pfaeffli, P. NVP-SRA880, a somatostatin sst_1 receptor antagonist promotes social interactions, reduces aggressive behaviour and stimulates learning. *Pharmacologist* **2002**, *44*, A254.

(32) Hoyer, D.; Nunn, C.; Hannon, J.; Schoeffter, P.; Feuerbach, D.; Schuepbach, E.; Langenegger, D.; Bouhelal, R.; Hurth, K.; Neumann, P.; Troxler, T.; Pfaeffli, P. SRA880, in vitro characterization of the first non-peptide somatostatin sst(1) receptor antagonist. *Neurosci. Lett.* **2004**, *361*, 132–5.

(33) Matrone, C.; Pivonello, R.; Colao, A.; Cappabianca, P.; Cavallo, L. M.; Del Basso De Caro, M. L.; Taylor, J. E.; Culler, M. D.; Lombardi, G.; Di Renzo, G. F.; Annunziato, L. Expression and function of somatostatin receptor subtype 1 in human growth hormone secreting pituitary tumors deriving from patients partially responsive or resistant to long-term treatment with somatostatin analogs. *Neuroendocrinology* **2004**, *79*, 142–148.

(34) Zatelli, M. C.; Tagliati, F.; Piccin, D.; Taylor, J. E.; Culler, M. D.; Bondanelli, M.; degli Uberti, E. C. Somatostatin receptor subtype 1-selective activation reduces cell growth and calcitonin secretion in a human medullary thyroid carcinoma cell line. *Biochem. Biophys. Res. Commun.* **2002**, *297*, 828–834.

(35) Zatelli, M. C.; Piccin, D.; Tagliati, F.; Bottoni, A.; Luchin, A.; Vignali, C.; Margutti, A.; Bondanelli, M.; Pansini, G. C.; Rosa Pelizzo, M.; Culler, M. D.; Degli Uberti, E. C. Selective activation of somatostatin receptor subtypes differentially modulates secretion and viability in human medullary thyroid carcinoma primary cultures: potential clinical perspectives. *J. Clin. Endocrinol. Metab.* **2006**, *91*, 2218−2224.

(36) Liapakis, G.; Hoeger, C.; Rivier, J.; Reisine, T. Development of a selective agonist at the somatostatin receptor subtype SSTR1. *J. Pharmacol. Exp. Ther.* **1996**, *276*, 1089–1094.

(37) Rivier, J. E.; Hoeger, C.; Erchegyi, J.; Gulyas, J.; DeBoard, R.; Craig, A. G.; Koerber, S. C.; Wenger, S.; Waser, B.; Schaer, J.-C.; Reubi, J. C. Potent somatostatin undecapeptide agonists selective for somatostatin receptor 1 (sst1). *J. Med. Chem.* **2001**, *44*, 2238–2246.

(38) Rivier, J. E.; Kirby, D. A.; Erchegyi, J.; Waser, B.; Eltschinger, V.; Cescato, R.; Reubi, J. C. Somatostatin receptor 1 selective analogues: 3. Dicyclic peptides. *J. Med. Chem.* **2005**, *48*, 515–522.

(39) Erchegyi, J.; Hoeger, C. A.; Low, W.; Hoyer, D.; Waser, B.; Eltschinger, V.; Schaer, J.-C.; Cescato, R.; Reubi, J. C.; Rivier, J. E. Somatostatin receptor 1 selective analogues: 2. *N*-Methylated scan. *J. Med. Chem.* **2005**, *48*, 507–514.

(40) Erchegyi, J.; Hoeger, C.; Wenger, S.; Waser, B.; Schaer, J.-C.; Reubi, J. C.; Rivier, J. E. *N*-Methyl scan of a sst1-selective somatostatin (SRIF) analog. In *Peptides—The Wave of the Future: 2nd International Peptide Symposium/17th American Peptide Symposium, San Diego, CA, June 10−14, 2001*; Lebl, M. , Houghten, R. A. , Eds.; Springer: Norwell, MA, 2001; pp719−720.

(41) Jiang, G.; Miller, C.; Koerber, S. C.; Porter, J.; Craig, A. G.; Bhattacharjee, S.; Kraft, P.; Burris, T. P.; Campen, C. A.; Rivier, C. L.; Rivier, J. E. Betidamino acid scan of the GnRH antagonist acyline. *J. Med. Chem.* **1997**, *40*, 3739–3748.

(42) Cervini, L.; Theobald, P.; Corrigan, A.; Craig, A. G.; Rivier, C.; Vale, W.; Rivier, J. Corticotropin releasing factor (CRF) agonists with reduced amide bonds and Ser7 substitutions. *J. Med. Chem.* **1999**, *42*, 761–768.

(43) Reubi, J. C.; Schaer, J.-C.; Wenger, S.; Hoeger, C.; Erchegyi, J.; Waser, B.; Rivier, J. SST3-selective potent peptidic somatostatin receptor antagonists. *Proc. Natl. Acad. Sci. U.S.A.* **2000**, *97*, 13973–13978.

(44) Erchegyi, J.; Wenger, S.; Waser, B.; Eltschinger, V.; Cescato, R.; Reubi, J. C.; Koerber, S. C.; Grace, R. C. R.; Riek, R.; Rivier, J. E. Use of betidamino acids in drug design. In *Understanding Biology Using Peptides, The 19th American Peptide Symposium, San Diego, CA, June 18−23, 2005*; Blondelle, S. E. , Ed.; Springer: Norwell, MA, 2005; pp517−518.

(45) Qasmi, D.; René, L.; Badet, B. An α-aminoglycine derivative suitable for solid phase peptide synthesis using Fmoc strategy. *Tetrahedron Lett.* **1993**, *34*, 3861–3862.

(46) Jiang, G.-C.; Simon, L.; Rivier, J. E. Orthogonally protected *N*-methyl-substituted α-aminoglycines. *Protein Pept. Lett.* **1996**, *3*, 219–224.

(47) Rivier, J. E.; Jiang, G.-C.; Koerber, S. C.; Porter, J.; Craig, A. G.; Hoeger, C. Betidamino acids: versatile and constrained scaffolds for drug discovery. *Proc. Natl. Acad. Sci. U.S.A.* **1996**, *93*, 2031–2036.

(48) Hoeger, C. A.; Galyean, R. F.; Boublik, J.; McClintock, R. A.; Rivier, J. E. Preparative reversed phase high performance liquid chromatography. II. Effects of buffer pH on the purification of synthetic peptides. *Biochromatography* **1987**, *2*, 134–142.

(49) Miller, C.; Rivier, J. Peptide chemistry: Development of high-performance liquid chromatography and capillary zone electrophoresis. *Biopolymers Pept. Sci.* **1996**, *40*, 265–317.

(50) Rivier, J.; Erchegyi, J.; Hoeger, C.; Miller, C.; Low, W.; Wenger, S.; Waser, B.; Schaer, J.-C.; Reubi, J. C. Novel sst$_4$-selective somatostatin (SRIF) agonists. Part I: Lead identification using a betide scan. *J. Med. Chem.* **2003**, *46*, 5579–5586.

(51) Miller, C.; Rivier, J. Analysis of synthetic peptides by capillary zone electrophoresis in organic/aqueous buffers. *J. Pept. Res.* **1998**, *51*, 444–451.

(52) Gairi, M.; Saiz, P.; Madurga, S.; Roig, X.; Erchegyi, J.; Koerber, S. C.; Reubi, J. C.; Rivier, J. E.; Giralt, E. Conformational analysis of a potent SSTR3-selective somatostatin analogue by NMR in water solution. *J. Peptide Sci.* **2006**, *12*, 82–91.

(53) Güntert, P.; Mumenthaler, C.; Wüthrich, K. Torsion angle dynamics for NMR structure calculation with the new program DYANA. *J. Mol. Biol.* **1997**, *273*, 283–298.

(54) Hagler, A. T. , Theoretical simulation of conformation, energetics and dynamics of peptides. In *The Peptides: Analysis, Synthesis, Biology*; Udenfriend, S., Meienhofer, J., Hruby, V. J. , Eds.; Academic Press: Orlando, FL, 1985; Vol. 7, pp213−299.

(55) Cescato, R.; Erchegyi, J.; Waser, B.; Piccand, V.; Maecke, H. R.; Rivier, J. E.; Reubi, J. C. Design and in vitro characterization of highly sst$_2$-selective somatostatin antagonists suitable for radiotargeting. *J. Med. Chem.* **2008**, *51*, 4030–4037.

(56) Hill, C. S.; Treisman, R. Differential activation of c-fos promoter elements by serum, lysophosphatidic acid, G proteins and polypeptide growth factors. *EMBO J.* **1995**, *14*, 5037–5047.

(57) Treisman, R. Journey to the surface of the cell: Fos regulation and the SRE. *EMBO J.* **1995**, *14*, 4905–4913.

(58) Nunn, C.; Cervia, D.; Langenegger, D.; Tenaillon, L.; Bouhelal, R.; Hoyer, D. Comparison of functional profiles at human recombinant somatostatin sst2 receptor: simultaneous determination of intracellular Ca^{2+} and luciferase expression in CHO-K1 cells. *Br. J. Pharmacol.* **2004**, *142*, 150–160.

(59) Reubi, J. C.; Schaer, J.-C.; Waser, B.; Hoeger, C.; Rivier, J. A selective analog for the somatostatin sst1-receptor subtype expressed by human tumors. *Eur. J. Pharmacol.* **1998**, *345*, 103–110.

(60) Hocart, S. J.; Jain, R.; Murphy, W. A.; Taylor, J. E.; Coy, D. H. Highly potent cyclic disulfide antagonists of somatostatin. *J. Med. Chem.* **1999**, *42*, 1863–1871.

(61) Hocart, S. J.; Jain, R.; Murphy, W. A.; Taylor, J. E.; Morgan, B.; Coy, D. H. Potent antagonists of somatostatin: Synthesis and biology. *J. Med. Chem.* **1998**, *41*, 1146–1154.

(62) Melacini, G.; Zhu, Q.; Osapay, G.; Goodman, M. A refined model for the somatostatin pharmacophore: conformational analysis of lanthionine-sandostatin analogs. *J. Med. Chem.* **1997**, *40*, 2252–2258.

(63) Grace, C. R. R.; Erchegyi, J.; Koerber, S. C.; Reubi, J. C.; Rivier, J.; Riek, R. Novel sst$_2$-selective somatostatin agonists. Three-dimensional consensus structure by NMR. *J. Med. Chem.* **2006**, *49*, 4487–4496.

(64) Bass, R. T.; Buckwalter, B. L.; Patel, B. P.; Pausch, M. H.; Price, L. A.; Strnad, J.; Hadcock, J. R. Identification and characterization of novel somatostatin antagonists. *Mol. Pharmacol.* **1996**, *50*, 709–715.

(65) Bass, R. T.; Buckwalter, B. L.; Patel, B. P.; Pausch, M. H.; Price, L. A.; Strnad, J.; Hadcock, J. R. Identification and characterization of novel somatostatin antagonists. *Mol. Pharmacol.* **1997**, *51*, 170 Erratum.

(66) Grace, C. R. R.; Erchegyi, J.; Koerber, S. C.; Reubi, J. C.; Rivier, J.; Riek, R. Novel sst$_4$-selective somatostatin (SRIF) agonists. Part IV: Three-dimensional consensus structure by NMR. *J. Med. Chem.* **2003**, *46*, 5606–5618.

(67) Grace, C. R. R.; Erchegyi, J.; Reubi, J. C.; Rivier, J. E.; Riek, R. ; Three-dimensional consensus of structure of sst$_2$-selective somatostatin (SRIF) antagonists by NMR. *Biopolymers* **2008**, *89* 1077−1087.

(68) Siehler, S.; Seuwen, K.; Hoyer, D. [^{125}I]Tyr^{10}-cortistatin14 labels all five somatostatin receptors. *Naunyn-Schmiedeberg's Arch. Pharmacol.* **1998**, *357*, 483–489.

(69) Siehler, S.; Seuwen, K.; Hoyer, D. Characterisation of human recombinant somatostatin receptors. 1. Radioligand binding studies. *Naunyn-Schmiedeberg's Arch. Pharmacol.* **1999**, *360*, 488–499.

(70) Fehlmann, D.; Langenegger, D.; Schuepbach, E.; Siehler, S.; Feuerbach, D.; Hoyer, D. Distribution and characterisation of somatostatin receptor mRNA and binding sites in the brain and periphery. *J. Physiol. (Paris)* **2000**, *94*, 265–281.

(71) Horiki, K.; Igano, K.; Inouye, K. Amino acids and peptides. Part 6. Synthesis of the Merrifield resin esters of N-protected amino acids with the aid of hydrogen bonding. *Chem. Lett.* **1978**, *2*, 165–168.

(72) Rivier, J. E.; Jiang, G.; Porter, J.; Hoeger, C.; Craig, A. G.; Corrigan, A. Z.; Vale, W. W.; Rivier, C. L. GnRH antagonists: novel members of the azaline B family. *J. Med. Chem.* **1995**, *38*, 2649–2662.

(73) Sypniewski, M.; Penke, B.; Simon, L.; Rivier, J. (*R*)-*tert*-Butoxycarbonylamino-fluorenylmethoxycarbonyl-glycine from (*S*)-Benzyloxycarbonyl-serine or from papain resolution of the corresponding amide or methyl ester. *J. Org. Chem.* **2000**, *65*, 6595–6600.

(74) Kaiser, E.; Colescott, R. L.; Bossinger, C. D.; Cook, P. I. Color test for detection of free terminal amino groups in the solid-phase synthesis of peptides. *Anal. Biochem.* **1970**, *34*, 595–598.

(75) Davis, D. G.; Bax, A. Assignment of complex ^{1}H NMR spectra via two-dimensional homonuclear Hartmann−Hahn spectroscopy. *J. Am. Chem. Soc.* **1985**, *107*, 2820–2821.

(76) Braunschweiler, L.; Ernst, R. R. Coherence transfer by isotropic mixing: application to proton correlation spectroscopy. *J. Magn. Reson.* **1983**, *53*, 521–528.

(77) Rance, M.; Sorensen, O. W.; Bodenhausen, B.; Wagner, G.; Ernst, R. R.; Wüthrich, K. Improved spectral resolution in COSY ^{1}H NMR spectra of proteins via double quantum filtering. *Biochem. Biophys. Res. Commun.* **1983**, *117*, 479–485.

(78) Kumar, A.; Wagner, G.; Ernst, R. R.; Wüthrich, K. Buildup rates of the nuclear Overhauser effect measured by two-dimensional proton magnetic resonance spectroscopy: implications for studies of protein conformation. *J. Am. Chem. Soc.* **1981**, *103*, 3654–3658.

(79) Macura, S.; Ernst, R. R. Elucidation of cross-relaxation in liquids by two-dimensional NMR spectroscopy. *Mol. Phys.* **1980**, *41*, 95–117.

(80) Macura, S.; Huang, Y.; Suter, D.; Ernst, R. R. Two-dimensional chemical exchange and cross-relaxation spectroscopy of coupled nuclear spins. *J. Magn. Reson.* **1981**, *43*, 259–281.

(81) Bax, A.; Davis, D. G. MLEV-17-based two-dimensional homonuclear magnetization transfer spectroscopy. *J. Magn. Reson.* **1985**, *65*, 355–360.

(82) Bothner-By, A. A.; Stephens, R. L.; Lee, J.; Warren, C. D.; Jeanloz, R. W. Structure determination of a tetrasaccharide: transient nuclear Overhauser effects in the rotating frame. *J. Am. Chem. Soc.* **1984**, *106*, 811–813.

(83) Güntert, P.; Dotsch, V.; Wider, G.; Wüthrich, K. Processing of multi-dimensional NMR data with the new software PROSA. *J. Biolmol. NMR* **1992**, *2*, 619–629.

(84) Eccles, C.; Güntert, P.; Billeter, M.; Wüthrich, K. Efficient analysis of protein 2D NMR spectra using the software package EASY. *J. Biomol. NMR* **1991**, *1*, 111–130.

(85) Wüthrich; K. In *NMR of Proteins and Nucleic Acids*; J. Wiley & Sons: New York, 1986.

(86) Koradi, R.; Billeter, M. MOLMOL: a program for display and analysis of macromolecular structures. *PDB Newsletter* **1998**, *84*, 5–7.

(87) Reubi, J. C.; Schaer, J. C.; Waser, B.; Wenger, S.; Heppeler, A.; Schmitt, J. S.; Mäcke, H. R. Affinity profiles for human somatostatin receptor sst1−sst5 of somatostatin radiotracers selected for scintigraphic and radiotherapeutic use. *Eur. J. Nucl. Med.* **2000**, *27*, 273–282.

(88) Reubi, J. C.; Kvols, L. K.; Waser, B.; Nagorney, D. M.; Heitz, P. U.; Charboneau, J. W.; Reading, C. C.; Moertel, C. Detection of somatostatin receptors in surgical and percutaneous needle biopsy samples of carcinoids and islet cell carcinomas. *Cancer Res.* **1990**, *50*, 5969–5977.

(89) Reubi, J. C. In vitro identification of vasoactive intestinal peptide receptors in human tumors: implications for tumor imaging. *J. Nucl. Med.* **1995**, *36*, 1846–1853.

(90) Baskin, D. G.; Wimpy, T. H. Calibration of [$_{14}$C]plastic standards for quantitative autoradiography of [^{125}I]labeled ligands with Amersham Hyperfilm beta-max. *Neurosci. Lett.* **1989**, *104*, 171–177.

(91) Miller, J. A.; Zahniser, N. R. The use of ^{14}C-labeled tissue paste standards for the calibration of ^{125}I-labeled ligands in quantitative autoradiography. *Neurosci. Lett.* **1987**, *81*, 345–350.

JM801314F